G.Melin and A.Girard
Département de Recherche Fondamentale sur la Matière Condensée
Laboratoire Plasmas et Sources d'Ions
C.E.A. Grenoble
38054 Grenoble Cedex 9, FRANCE

Abstract

ECR ion sources (ECRIS), an outgrowth of the fusion plasma research, keep regularly improving and expanding since the pioneer time of the first facilities about twenty years ago. For multiply charged ions, both gases and metals, ECRIS are known to be highly reliable, low cost technology devices, which can deliver intermediate charge states, high intensity ion currents in continuous mode of operation (as high as 0.5 eμA of U^{43+} !). The basic principles of ECRIS operation are here presented, as well as the underlying atomic physics and plasma physics, and the way they are modeled. The design, main features and performances of existing ECRIS are then examined. At last the present trends of development, and what could be an advanced concept for an ECRIS, are discussed.

The Electron Cyclotron Resonance Ion Sources (ECRIS) are issued from fusion plasma machines, the so-called open-ended mirror machines [1] initially built for their plasma confinement properties. It is amazing to notice that the today ECRIS, which are small mirror machines, are optimized for their ion loss rates, e.g. the ion currents to be extracted. This remark reveals the basic compromise that ECR sources of multiply charged ions (MCI) have to face, good confinement and high losses both optimized ! This contradictory situation is discussed below.

The ECRIS for MCI have been invented and developed by R.Geller and his coworkers about twenty years ago [2]. The accelerators, essentially cyclotrons, together with the Grenoble group contributed to their present status, but an increasing number of small scale facilities for atomic physics experiments are now utilizing ECRIS, and are concerned by their development; they also have applications for surface treatment, ion implantation, etc... The ECRIS can deliver high charge state, high intensity ion beams in continuous regime of operation usually with good stability; they can run over a wide range of ion species, with reliability and longevity (no cathode, no filament). They are easy to handle, to operate and to repair, their rather simple technology and their low cost make them quite attractive.

In ECRIS the production of high charge state ions is made through the confinement of a hot electron plasma, and not directly controlled as in electron beam ion sources (EBIS). This situation where both plasma physics, atomic physics, and to a lesser extent surface physics, get simultaneously involved, makes ECRIS behavior and data interpretation somewhat confusing as many parameters play a role in the ion production. Although this contributed to render them difficult to understand, not to say mysterious, many progresses have been achieved both in the understanding of the ECRIS physics and theory, and in the performance improvement. However as explained below, there are still some ECRIS parameters whose control remains difficult and not well understood, this may give rise to differences of understanding or recipes among the numerous users of ECRIS.

1.3.2 Basic principles of ECRIS operation

The ECRIS is an open-ended magnetic trap, which basically confines a hot electron plasma. The electrons heated by interaction with rf waves are magnetically confined. They are moving back and forth along the magnetic field lines, and thus undergo a large number of oscillations through the configuration, while the ions get progressively ionized by electron impact.

Thus basically the system has the property of confining a plasma. Its main ingredients are:

(i) the magnetic configuration,

(ii) the heating of electrons by rf waves at the cyclotron frequency, i.e.

$$\omega_{ce} = \frac{e\,|B|_{res}}{m_e} = \omega_{rf} \ , \qquad (1)$$

(iii) the necessary sources of electrons, which allow the electron density to build up in the trap.
As compared to EBIS, the ECRIS do not have a direct control of parameters such as electron energy, ion confinement; these are only indirectly controlled by external knobs, limited in number and not univocal, such as rf power, pressure, magnetic field, rf frequency. But the main advantage of ECRIS with respect to EBIS is the multi-use of the same electrons for enhancing the ionization, which results from the electron confinement.
The extracted ion current I_q of charge state q at one end of an ECRIS is equal to the ion loss rate of the ECRIS trapped plasma:

$$I_q \simeq \frac{1}{2}\frac{n_q\, qeV_x}{\tau_q} \ , \qquad (2)$$

here the coefficient $\frac{1}{2}$ means that the magnetic configuration has two symmetrical ends, usually called extraction and injection, n_q is the density of the ion of charge state q, τ_q the confinement time of this ion; V_x is the part of the hot plasma volume that maps along the magnetic field lines into the extraction area. Assuming the plasma charge neutrality

$$n_e = \sum_q n_q\, q \ , \qquad (3)$$

n_e being the electron density, one may also expect,

$$I_q \propto n_e V_x \ . \qquad (4)$$

The formula (2) that gives the intensity (I_q) of a given ion charge state (q) delivered by the ECRIS, brings up in itself some contradiction:
(i) on one hand high charge state (q) ions require long τ_q because of the ionization times, which in turn means that the losses (I_q) cannot be very large,
(ii) on the other hand high losses (high I_q) evidently would not allow the plasma density (n_q and n_e) to build up, which would seriously reduce the ionization efficiency in order to produce high charge state(q) ions.
This situation results from the self-consistent aspect of a plasma confinement machine. Fortunately owing to the large number of parameters involved in ECRIS operation, some compromise is possible and by means of the knobs mentioned above, one can match the ionization time to the ion confinement time for the desired ion. This tuning is always necessary in ECRIS, and is different for every ion.

1.3.2.1 Magnetic configuration

R.Geller [2] and his coworkers [3] definitely contributed to the ECRIS development as follows:
(i) a hot electron mirror machine with hexapolar minimum-B is utilized in order to produce multiply charged ions.

in order to obtain high charge state ions.
(iii) the source is miniaturized by using permanent magnets for the hexapolar minimum-B (the Supermafios hexapole [2], made of six conductors, had a power consumption as large as 2.5 MW !).
Most ECRIS keep this initial design, as sketched in figure 1, of a mirror field created by two sets of coils combined with a radial hexapolar field, that gives the magnetic flux tubes the shape of the one shown in figure 2a (when mapping the plasma center to one end of the device). The resonance surface, as defined by (1), egg-shaped with azimuthal hexapolar modulations, lies at the center and confines the rf heated electrons as shown in figure 2b [4]. The hot electron plasma volume V_p is approximately limited by this surface, as experimentally proved by using a movable probe while monitoring the X-ray flux [5].
In ECRIS, like in mirror machines, the electrons spiral around the magnetic field lines and are confined in the radial direction (or perpendicular $\perp$). Axial confinement (or parallel $\|$) occurs because the magnetic field increases at each end of field lines. The electron confinement results from the conservation of (i) its magnetic moment μ_e and (ii) its total energy E_e, outside the ECR zone of heating, during its motion along the field line,

$$\mu_e = \frac{\frac{1}{2}m_e v_\perp^2}{|B|} \quad , \quad E_e = \frac{1}{2}m_e \left(v_\perp^2 + v_\|^2\right) \quad ,$$

here $v_\perp$ and $v_\|$ are the perpendicular and parallel components of the electron velocity. Therefore the electrons are reflected within the configuration, i.e. when $v_\| = 0$, if their velocity angle $\tan^{-1}(v_\perp/v_\|)$ at the minimum magnetic field B_{min} exceeds the so-called "loss cone" angle $\sin^{-1}(B_{min}/B_{max})^{1/2}$ [1].
The equal $|B|$ surfaces of such a magnetic configuration, mirror field and multipolar minimum-B (usually hexapolar), are closed and nested in each other from the center of the configuration (figure 2c), the resonance surface (equal $|B|_{res}$) being one of these surfaces. Regarding the plasma equilibrium, i.e. the confinement capability of this configuration, it can be demonstrated [6] that the equal $|B|$ surfaces (magnetic isobars) are also equal plasma pressure surfaces (plasma isobars). Thus the plasma is confined only within closed magnetic isobars: when such a magnetic isobar surface touches the walls, the plasma is no longer confined. Therefore if $|B|_{last}$ is the highest $|B|$ value corresponding to a closed equal $|B|$ surface, the higher $|B|_{last}$, the better the confinement. This criterion appears to be satisfied in the high performance ECRIS. It should be clearly stressed that the magnetic isobars are not magnetic field line envelopes. The particles (essentially electrons) follow the field lines while moving through the magnetic configuration, this allows to collect particles (electrons and ions) at the ends of the machine. The field lines are not closed and hit the walls (figure 2a), the plasma pressure is not constant along the field lines, it is anisotropic owing to the cyclotron motion of particles. Although the relationship between the plasma pressure and the magnetic pressure $|B|^2/2\mu_0$ is not straightforward, it can be shown that the anisotropic plasma pressure depends only upon $|B|$.

the inward curvature of the magnetic field lines (figure 2a), was early proved to be necessary for magneto-hydro-dynamic (MHD) stability with respect to interchange modes [1].

1.3.2.2 Electron cyclotron heating

Considering the cyclotron heating of electrons in a magnetic configuration as defined above, one has to deal with two different aspects that are separately analyzed in this section, the particle behavior during the heating process, and the rf waves to be used for heating that propagate in ECRIS plasmas.

1.3.2.2.1 electron behavior

The electron cyclotron heating plays an intrinsic role in the electron confinement. In the single particle approximation, the electron moving back and forth along the magnetic field lines receives kicks (+ or −) of transverse velocity from the rf electric field while crossing the resonances (figure 3). Its phase in the cyclotron motion, with respect to the rf wave becomes random. The theory predicts a stochastic heating limited at high energy by adiabatic invariants [7].
The electron heating can be modeled as a diffusion process in velocity space. Thus the electron distribution function (EDF) of the ECRIS plasma may be calculated from a Fokker-Planck equation [8] as the result of the combined effect of this diffusion and of Coulomb collisions; these collisions lead to electron losses through pitch angle scattering. The EDF is expected to be non-maxwellian, with a high energy tail. Experimental measurements confirm this prediction (see below).

1.3.2.2.2 rf waves in ECRIS

In ECRIS plasmas, despite the electron heating, the cold plasma and Appleton-Hartree (electron waves) approximations are still valid, and the main ECRIS plasma waves are [9]:
• in parallel or quasi-parallel propagation (wave vector **k** parallel to **B**): the whistler wave (electric field circularly polarized, perpendicular to **k**), and a high frequency wave, sometimes called the maser wave.
• in perpendicular or quasi-perpendicular propagation (wave vector **k** perpendicular to **B**): the O wave (electric field linearly polarized, perpendicular to **k**, and parallel to **B**), and the X wave (electric field elliptically polarized in the plane perpendicular to **B**).
The preferential wave to be used is the whistler wave, having a right handed circularly polarized electric field that rotates in the electron gyromagnetic direction; this wave carries the rf power to the cyclotron resonance $\omega_{rf} = \omega_{ce}$ where it normally couples to the electrons. The fraction of the rf power not absorbed at the cyclotron resonance, owing to reflections either on cut-offs [9] or on the chamber walls, may also be absorbed as an X wave at the so-called upper hybrid resonance,

$$\omega_{rf} = \omega_{uh} = \left(\omega_{ce}^2 + \omega_{pe}^2\right)^{1/2} \quad . \tag{5}$$

$$\omega_{pe} = \left(\frac{n_e e^2}{m_e \epsilon_0}\right)^{1/2} \simeq 2\pi \times 9000.\sqrt{n_e} \leq \omega_{rf} \quad (2\pi\text{Hz, cm}^{-3}), \qquad (6)$$

($\omega_{pe}/2\pi$ is the so-called electron plasma frequency, and the electron density corresponding to $\omega_{pe} = \omega_{rf}$ is often referred to as the *cut-off* electron density),
which was suggested by the plasma shielding of rf waves [2], is only the cut-off of the O wave, usually not excited in ECRIS. However this cut-off has been often referred to for the ECRIS maximum performance [2] to give the scaling, with using formula (4),

$$(I_q)_{\max} \propto \omega_{\text{rf}}^2 \ , \qquad (7)$$

which has not been yet proved.
In the ECRIS plasma depending upon the vacuum wavelenght of the wave being launched for heating, two limiting cases have to be considered:
- $\lambda_0 <$ plasma dimensions:
Assuming that the plasma parameters (electron density n_e and magnetic field $|B|$) are constant, one can calculate the dispersion relation of the plasma waves (i.e. the conditions of wave propagation), $D(\omega, k_\perp, k_{||}) = 0$, and make the ray tracing of the wave into the plasma from the antenna, in order to evaluate the electric field, the heating and the absorption.
- $\lambda_0 \simeq$ plasma dimensions:
Electromagnetic (em) cavity effects dominate because of boundary conditions, and the em field is not localized and has a spatial distribution. Although many em modes may exist [10] (multimode cavity), they may be selected depending upon the rf coupling system [11]. Most of the existing ECRIS have to deal with eigenmodes: eigenmodes of a cylindrical cavity, $TE_{m,n,p}$ or $TM_{m,n,p}$ (the indexes stand respectively for the ψ azimuthal, r radial, and z axial or parallel coordinates), are actually standing waves formed by oblique waves with respect to the parallel direction, as their dispersion relation in vacuum can always be written in the form,

$$k_0^2 = k_\perp^2(\text{m,n}) + k_{||}^2(\text{p}) \ ,$$

where k_0 is the vacuum wave number. Thus the excitation of plasma waves with the $k_\perp$ and $k_{||}$ components of the selected eigenmode, has to be considered accordingly. Usually this excitation is quasi-parallel, because $k_{||} \gg k_\perp$, owing to the dimensions of the ECRIS plasma chambers, and the rf power is coupled to the whistler wave.

1.3.2.3 Electron sources

Supplying cold electrons to the ECRIS magnetic trap is a necessary condition to obtain an electron density large enough for efficient ionization. Remarkable improvements were achieved by using different methods, either from external sources or from internal sources [12][13].
- external sources: (i) 1st stage, an auxiliary ECR discharge, which in the early sources was considered to be important for the singly charged

to be the essential role of the 1st stage [14]. (ii) the plasma cathode being developed at Riken [12] is actually a 1st stage with an electrode for electron extraction at low energy and injection into the main stage. (iii) a low voltage electron gun was used on the AECR source [15]; the effect was quite impressive in the performance, but the gun cathode had a limited life-time.

- internal sources: (i) multi-ionization of atoms is of course a permanent source of new cold electrons, however it cannot sustain by itself the total electron density. (ii) convenient coatings having a high yield for secondary electrons on the ECRIS walls, e.g. ThO_2 [2], SiO_2 [15], or Al_2O_3 [16], prove to be very efficient; however under the impact of plasma particles, these coatings need to be frequently regenerated, except for Al_2O_3. (iii) a negatively biased disk or probe reduces the plasma electron losses and/or provides new electrons from secondary emission of impinging plasma particles [14][17]. Recent data [13] show that the internal sources by wall coating may have another interesting effect of lowering the plasma potential (see below).

The permanent refueling of cold electrons in the ECRIS by these electron sources compensates for the electron losses caused by the various loss mechanisms of the confined plasma.

1.3.3 Atomic physics and plasma effects – ECRIS modeling

As described below in ECRIS modeling, the production of a given ion charge state in ECRIS obeys a balance equation between (i) the rates of production and losses of this ion allowed by atomic physics processes (ionization, charge exchange, etc...), and (ii) the rates of losses caused by the imperfect ion confinement in the magnetic configuration (which are nonetheless necessary for the extracted ion beam of this charge state). Roughly speaking, atomic physics processes balance the plasma physics effects, both are described in this section.

1.3.3.1 Main atomic physics processes in ECRIS

The step by step ionization of atoms by electron impact, or successive ionization, is by far the dominant ionization process in ECRIS. The rate of ionization by electrons of an ion from charge state $(q-1)$ to charge state (q) is calculated from the ionization cross-sections after averaging over the plasma EDF, usually considered as a Boltzman distribution of temperature T_e for the sake of simplicity. The cross-sections are given by the Lotz formula [18]. The result of the integration over the EDF gives the rates of ionization, as shown for example on figure 4 for argon gas. The coefficients of the Lotz formula are however known only for few elements, the usual and noble gases, with a reasonable accuracy. Another mechanism of single ionization may also occur in two steps, excitation and subsequent decay by auto-ionization. An experimental evidence of the sequential ionization is found with metallic ions by rf pulsing, while

The multiple step ionization $(q-n)$ to (q), sometimes called shake-off ionization, may substantially reduce the ionization times in a specific electron energy range; however, once averaged over the EDF, this mechanism remains negligible. Orders of magnitude of these ionization cross-sections can be found in the comprehensive data compilation of H.Tawara and T.Kato [20].

Another mechanism of ionization by electron impact in ECRIS is the Auger effect. High energy electrons may directly produce a K shell vacancy in the atom, which by Auger effect may be followed by a double vacancy in the L shell, soon followed by twice more holes in the M shell and so on (Auger cascade effect [21]). This remarkable effect is observed by X ray spectroscopy of the ECRIS plasma, for example while monitoring the K_α and K_β lines of krypton at different input rf powers [5]:

- at very low rf power (a few watts), the characteristic K line of neutral or quasi-neutral krypton is already observed, which means that electrons energetic enough (~15 keV) are already existing.
- the K line FWHM increases with rf power: this indicates that all states of krypton ions with one K vacancy and many L vacancies (K^1L^n states) are produced.

Although remarkable this mechanism which would be efficient only for high-Z atoms, cannot account for a significant part of the ionization.

The recombination process is the reverse of ionization and consists of a capture by an ion of a free electron. The excess of energy is removed by the emission of one photon (radiative recombination, binary collision of one electron and a multicharged ion), or several photons (dielectronic recombination, absorption by an ion of an energetic electron with elevating a bound electron to an excited state). Although important only at high charge states, the latter mechanism, dielectronic recombination, dominates over the former; however, for plasma densities so far involved in ECRIS ($n_e \leq$ a few 10^{12}cm^{-3}), even dielectronic recombination appears not to be important.

The charge exchange effect, usually considered as the limiting mechanism for high charge states, may be seriously reduced by the burn-up effect of neutrals in the ECRIS plasma, which means that dimension effects may be important: large dimension ECRIS may allow the formation of a central core plasma where the density of neutrals is so low that charge exchange processes become negligible. Thus charge exchange is only important to some extent in today ECRIS. Regarding charge exchange effects between different ions, either in charge states and/or in species, few experimental data exist, but globally they are not so important.

1.3.3.2 Plasma effects in ECRIS

ECRIS are subject to specific laws of plasma confinement, which determine the rates of losses, i.e. the currents of ions and electrons, that can be extracted. They are summarized in this section.

As a result of the electron cyclotron heating, the EDF that develops in ECRIS can be divided in two electron populations, both maxwellian for the sake of simplicity: bulk electrons of temperature from a few hun-

and tail electrons with temperature of several tens of keV (figure 7). Tail electrons, or high energy electrons, are definitely existing in ECRIS, as proved by different measurements (bremsstrahlung X-rays, electron cyclotron emission, diamagnetism) [22][23][24]. However in the coming sections, only one population of electrons is considered, bulk maxwellian electrons of temperature T_e and density n_e for simplicity.

1.3.3.2.1 ambipolar potential

In ECRIS a positive potential ϕ (a few tens of volts) with respect to the walls, is usually observed. This ϕ potential has to be compared with that of a sheath between a wall and a plasma [25]. The colder electrons of ECRIS leave the plasma faster than the ions. The potential ϕ appears in order to accelerate the ions and to retard the electrons, so that the total current at the walls is zero. It may be experimentally measured from the ion beam energy with mass spectrometry as shown in figure 8 [13]. The plasma potential ϕ strongly depends upon the ion density charge state distribution (CSD) in the ECRIS: the high charge of ions partially compensates for their low mobility, so that ECRIS delivering higher charge state ions have a lower plasma potential. A low plasma potential source is also expected to reduce some non desirable effects: a lower sputtering of the wall material in the source, and a better emittance. Thus the plasma potential control may become for ECRIS an important issue. Actually the plasma potential along the axis of the ECRIS confinement region would be a positive potential hill ϕ with a small negative well $\Delta\phi$ located at the center, i.e. on the top of this hill (figure 9). This small dip of potential $\Delta\phi$ (perhaps only a few volts at the most), could be created by the high energy electrons magnetically confined, it is going to be very important for the ion confinement.

1.3.3.2.2 electron and ion confinement

Without complete solutions of the Fokker-Planck equation [8], which would give the EDF in mirror geometry with electron cyclotron heating and Coulomb collisions, averaged parameters of the electron confinement can be calculated under some approximations: maxwellian EDF non-anisotropic, only the perpendicular velocity component is considered (resulting from the heating effect), electrons of energy lower than that of the ambipolar potential, $e\phi$, cannot be lost.
The electron particle confinement time τ_e is defined as the ratio of the total electron density, and the number of electrons lost per unit time and per unit volume by Coulomb scattering into the the loss cone at the rate given by Spitzer [26]. Utilizing the Spitzer 90° collision frequency [26], an upper estimate of τ_e for ECRIS can be obtained in the limit $e\phi/kT_e \ll 1$,

$$\tau_e \simeq 4.6\,10^3 \frac{T_e^{3/2}}{n_e\, q_{\text{eff}}} \sqrt{\frac{\phi}{T_e}} \text{ (s, eV, cm}^{-3}\text{, V)} , \qquad (8)$$

$q_{\text{eff}} = \sum n_q q^2 / n_e$ is the mean effective ion charge. Here only the dominant electron-ion collisions are taken into account.

of the total electron energy content, and the electron energy lost per unit time and per unit volume by Coulomb scattering into the loss cone. With the same approximations and limit $e\phi/kT_e \ll 1$, an upper estimate of τ_{T_e} is given by

$$\tau_{T_e} \simeq 5.2\,10^3 \frac{T_e^{3/2}}{n_e\, q_{\text{eff}}} \text{ (s, eV, cm}^{-3}) \,, \tag{9}$$

The difference between these two formulas (8) and (9), i.e. the dependence of the plasma potential ϕ, simply means that the low energy electrons, close to $e\phi$ in energy, have an important contribution to the total particle losses, but their contribution to the total energy losses is small. The formulas (8) and (9) do not depend upon the mirror ratio $R = B_{max}/B_{min}$ as they used the Spitzer 90° collision frequency, this means that the electrons in the $(v_\perp, v_\parallel)$ space are supposed to be localized near the $v_\perp$ axis and that they experience 90° scattering deflections which put them on the $v_\parallel$ axis, the loss cone angle being zero. Previous Fokker-Planck computer calculations of collisional losses of light ions for fusion plasma confinement have shown that the mirror ratio dependence of the confinement time of these light ions can be fitted by a function $\log_{10} R$ [27]. Perhaps such a function could be included in formulas (8) and (9) in order to account for the mirror ratio effect, even for heavy ions, but this has not been calculated. Nonetheless as given here these formulas are upper values of the corresponding confinement times.
As explained below in ECRIS modeling, a rough power balance of the ECR discharge in steady state can be written as, P_{abs} being the absorbed rf power,

$$\frac{P_{\text{abs}}}{V_p} \simeq \frac{n_e k T_e}{\tau_{T_e}} \,,$$

where V_p is the plasma volume. Thus the classical coulomb scattering losses allows an electron density scaling,

$$n_e \propto \sqrt{\frac{P_{\text{abs}}}{V_p}}\, T_e^{1/4} \,, \tag{10}$$

which, with using formula (4), may explain the observed extracted ion current behavior as a function of the rf power (figure 10).
However kinetic instabilities [28] that make the ECR discharge running unstable, may reduce the actual electron energy confinement time to a value lower than the classical value given by formula (9). This may cause a performance saturation [8][29].

The ion confinement time τ_q in the ECRIS plasma strongly depends upon the ion collisionality, i.e. the number of ion-ion collisions that the ion may experience during each bounce through the ECRIS plasma. This collisionality is therefore given by the ratio of the bounce time τ_b,

$$\tau_b \simeq \frac{l}{v_{T_i}} \text{ with } v_{T_i} = \sqrt{\frac{2kT_i}{A_i\, m_p}} \text{ and } A_i = \frac{m_i}{m_p} \,,$$

the ion and proton masses, to the ion-ion scattering time τ_{ii}, which is given by the Spitzer 90° scattering time [26] for the ion of charge state q and mass ratio A_i as follows,

$$\frac{1}{\tau_{ii}} = \sum_j \frac{1}{\tau_{ij}} \simeq 4\pi e^4 \frac{n_e\, q^2 q_{\rm eff} \ln\Lambda}{A_i^{1/2} m_p^{1/2} k T_i^{3/2}} \quad \text{(cgs units)},$$

in practical units, with $\ln\Lambda = 10$

$$\tau_{ii} \simeq 1.1 \frac{A_i^{1/2} T_i^{3/2}}{n_e\, q^2 q_{\rm eff}} \quad \text{(s, eV, cm}^{-3}\text{)}.$$

The ion temperature T_i is considered to be the same for all charge states and species owing to the large ion-ion collision frequency. Depending upon the ion collisionality, the following expressions for the ion confinement time have to be considered [30],

• $\tau_{ii} \gg \tau_b$, i.e. in non collisional confinement, the Pastukhov formula prevails [31],

$$\tau_P = \frac{\sqrt{\pi}}{2} \ln(2R+2) \frac{qe\,\triangle\,\phi}{kT_i} \frac{R+1}{R} \frac{\exp\left(\frac{qe\triangle\phi}{kT_i}\right)}{1+\frac{qe\triangle\phi}{2kT_i}} \tau_{ii} \quad . \tag{11}$$

• $\tau_{ii} \sim \tau_b$, i.e. in moderately collisional confinement, the flow formula prevails,

$$\tau_f \simeq Rl \sqrt{\frac{A_i m_p}{kT_i}} \exp\left(\frac{qe\,\triangle\phi}{kT_i}\right) \quad . \tag{12}$$

• $\tau_{ii} \ll \tau_b$, i.e. in highly collisional confinement, the diffusion formula prevails,

$$\tau_D \simeq \frac{a^2}{D_i} \text{ with } D_i = \frac{kT_i}{m_i\,\nu_{ii}} \simeq v_{T_i}^2 \tau_{ii} \quad , \tag{13}$$

here a is the smallest characteristic plasma dimension (plasma diameter). Practically the final expressions for the ion confinement τ_q may be taken as follows,

- if $\tau_{ii} \geq \tau_b$, the ion *feels* the magnetic field as well as the potential well $\triangle\phi$ and,

$$\tau_q \simeq \tau_P + \tau_f \quad ,$$

most of the ions of today ECRIS are likely in a regime where $\tau_q \simeq \tau_f$.

- if $\tau_{ii} \ll \tau_b$, the ion does not *feel* the magnetic field and,

$$\tau_q \simeq \tau_D \quad ,$$

the question whether this formula should also include the effect of the potential well $\triangle\phi$ is still open, but this regime only applies to very highly charged ions.

The ECRIS in pulsed mode can deliver higher intensities of highly charged ions during the afterglow plasma [5][32]. Turning the rf power off causes the electron population to collapse rapidly because of (i) a decrease of the electron temperature T_e as the electron heating does not exist any longer, and (ii) a reduction of some electron sources, such as the secondary emission from hot electrons impinging on the walls. The confined highly charged ions are compelled to leave the plasma because of charge neutrality. Thus the ion loss rate, and the extracted ion intensity may increase for a short time, owing to a different compromise between intensity and charge state as discussed earlier.
Impressive extracted intensities have been obtained, as much as 100eμA of Bi^{28+} [33] and Pb^{28+} [32], 30eμA of Au^{27+} [29] (figure 11), i.e. a few pμA of these metallic ions in pulses a few ms long at a frequency of a few tens Hz.

1.3.3.2.4 gas mixing

In order to obtain higher charge states, a carrier gas is generally used in ECRIS with the main element (gas or metal) to be ionized, the density of this carrier gas is dominant with respect to that of the other element, and the carrier gas mass is always lower. Various interpretations have been proposed, none of them is fully satisfactory: (i) a dilution effect lowering the mean ion charge (q_{eff} defined earlier) and reducing the electron loss rates according to the formulas (8) and (9) [2]; (ii) an increase of the electron density because of the better ionization efficiency of the carrier gas, the conditions (n_e, T_e) of the ECRIS plasma with carrier gas being more favorable to the desired multicharged ion production [34]; (iii) the ion cooling which results from the mass effect in the ion-ion collisions between the two species [35][36]: it lowers the ion temperature T_i and increases the ion confinement time of highly charged states as shown by the formulas (11) to (13). Oxygen, nitrogen and helium are the most usual gases for this experimental technique. However gas mixing does not always work out, especially in high performance sources [37].
A remarkable experiment referred to as oxygen anomaly [36] indicates that at least a mass effect is present in gas mixing: a mixture consisting of three oxygen isotopes, masses $A = 18$ (32.9%), $A = 17$ (51.2%) and $A = 16$ (15.9%) is utilized. The anomaly is that the extracted current ratio I_q^{O18}/I_q^{O17} increases with the charge state q: at high charge state this current ratio (0.78 at $q = 7$) is larger than the initial mixture ratio (0.64), whereas at low charge state this ratio (0.58 at $q = 3$) is lower than the initial mixture ratio. When introducing He4 gas in this oxygen mixture, the anomaly is reduced. The explanation is still puzzling, but both mass and charge state play a role likely through the ion confinement time.

1.3.3.3 ECRIS modeling

ECRIS modeling has been undertaken since long as far back as the first ECRIS [38][39][40], the CSD of the extracted currents being often the

unknown inputs, the fitting of experimental CSD by codes has been often relatively good, although over a limited range of variation of the parameters. This is likely because many internal variables are distribution-averaged (in space, velocity, etc...) so that the ion loss rates, i.e.the extracted ion currents are not varying rapidly when changing the external knobs, pressure, magnetic field, rf power, etc..., except for bursting phenomena such as kinetic instabilities. But still the relationships between these external knobs and the internal variables n_e, T_e, n_q $(q = 1, q_{max})$, n_0 (neutral density), T_i, τ_q, τ_e, τ_{T_e}, ϕ, $\Delta\phi$, etc..., are not straightforward and simple scaling laws that would summarize the physics of ECRIS seem quite difficult, but impossible, to establish.

The atomic data are the best known inputs, at least for most gases and medium Z elements. Like the first codes, the recent ones [6][30][41] describe the time evolution of the particle densities, thus using a fluid approximation (integrated parameters) in a 0 D model (no spatial dimension); maxwellian velocity distribution functions are usually considered (for simplicity), however a theoretical work for using actual solutions of the EDF equation with the rf heating term has been recently undertaken [8]. Some effects are ignored or not correctly described: gas mixing, electron sources, plasma-wall interactions, diamagnetic effect of hot electrons, etc... None of these codes is self-consistent.

The plasma physics description as given above seems to be correct for τ_e and τ_q, although the ion confinement time τ_q may be not as optimistic as that given by the above formulas. For the atomic physics description the step by step ionization by electron impact and the charge exchange with neutrals are the two only considered mechanisms. The evolution as a function of the charge state q of these three dominant mechanisms, plasma confinement, step by step ionization and charge exchange, explains the peaked shape of the observed CSD (for instance see argon CSD in figure 12) which is generally fairly well simulated in steady state $(\frac{d}{dt} = 0)$. The main equations of ECRIS modeling are as follows:

• neutral density inside the plasma (n_0),

$$\frac{dn_0}{dt} = \frac{\frac{Q_0}{kT_0} - n_0 S_p}{V} - n_e < \sigma v >_{0\to 1}^{ion} n_0 - n_0 \sum_{q=2}^{q_{max}} < \sigma v >_{q\to q-1}^{cx} n_q \quad , \quad (14)$$

Q_0 is the total input neutral flow rate and S_p the pumping speed of the pumping system in the plasma chamber of volume V (Q_0 and S_p usually expressed respectively in torr.liter/s and liter/s as practical units), T_0 is the temperature of neutrals (equal to the room temperature).

• electron population (n_e, T_e),

$$\frac{dn_e}{dt} = S_e + n_e \sum_{q=0}^{q_{max}-1} < \sigma v >_{q\to q+1}^{ion} n_q - \frac{n_e}{\tau_e} \quad , \quad (15)$$

S_e (number of electrons per unit plasma volume) stands for the external electron sources.

$$\frac{d\,(n_e T_e)}{dt} = \frac{P_{abs}}{V_p} - \frac{n_e T_e}{\tau_{T_e}} - n_e \nu_{ei}\,(T_e - T_i) - P_{ion} \quad , \quad (16)$$

two terms are by far dominant, the third term is the electron-ion power transfer which results from the electron-ion collision frequency ν_{ei} and which is the ion heating term. Owing to the large difference between ion and electron masses, this collisional heating is not very efficient, T_i is only of the order of 1 eV and $T_i \ll T_e$; in practical units ν_{ei} writes,

$$\nu_{ei} \simeq 3.2\,10^{-9}\frac{n_e\, q_{\rm eff}\, \ln\Lambda}{A_i\, T_e^{3/2}} \quad (\mathrm{s}^{-1},\ \mathrm{cm}^{-3},\ \mathrm{eV}).$$

P_{ion} is the power consumed for ionization.

• ion population (n_q, $q = 1, q_{max}$, T_i),

$$\frac{dn_1}{dt} = S_1 + n_e <\sigma v>^{ion}_{0\to 1} n_0 - n_e <\sigma v>^{ion}_{1\to 2} n_1 + n_0 \sum_{q=2}^{q_{max}} <\sigma v>^{cx}_{q\to q-1} n_q + n_0 <\sigma v>^{cx}_{2\to 1} n_2 - \frac{n_1}{\tau_1} \quad , \tag{17}$$

S_1 stands for an external monocharged ion source (for example the 1rst stage of the source).

$$\frac{dn_q}{dt} = + n_e <\sigma v>^{ion}_{q-1\to q} n_{q-1} - n_e <\sigma v>^{ion}_{q\to q+1} n_q + n_0 <\sigma v>^{cx}_{q+1\to q} n_{q+1} - n_0 <\sigma v>^{cx}_{q\to q-1} n_q - \frac{n_q}{\tau_q} \quad , \tag{18}$$

$$\frac{dn_{q_{max}}}{dt} = + n_e <\sigma v>^{ion}_{q_{max}-1\to q_{max}} n_{q_{max}-1} - \frac{n_{q_{max}}}{\tau_{q_{max}}} - n_0 <\sigma v>^{cx}_{q_{max}\to q_{max}-1} n_{q_{max}} \quad , \tag{19}$$

$$\sum_{q=1}^{q_{max}} \frac{d\,(n_q T_i)}{dt} = n_e \nu_{ei}\,(T_e - T_i) - \sum_{q=1}^{q_{max}} \frac{n_q T_i}{\tau_{T_i}} \quad , \tag{20}$$

τ_{T_i} would be the ion energy confinement time.

In steady state ($\frac{d}{dt} = 0$), a few simplified relationships may be obtained,

• particle balance from the sum of ion density equations,

$$\frac{\frac{Q_0}{kT_0} - n_0 S_p}{V} = \sum_{q=1}^{q_{max}} \frac{n_q}{\tau_q} - S_1 = n_0 (n_e <\sigma v>^{ion}_{0\to 1} + \sum_{q=2}^{q_{max}} <\sigma v>^{cx}_{q\to q-1} n_q) \quad ,$$

which can be written with a good approximation as,

$$\frac{\frac{Q_0}{kT_0} - n_0 S_p}{V} = \sum_{q=1}^{q_{max}} \frac{n_q}{\tau_q} - S_1 \simeq n_0 n_e <\sigma v>^{ion}_{0\to 1} \quad . \tag{21}$$

• charge balance,

$$\frac{n_e}{\tau_e} + S_1 = \sum_{q=1}^{q_{max}} \frac{q\, n_q}{\tau_q} + S_e \quad . \tag{22}$$

set of equations, while neglecting S_1 and considering that

$$\sum_{q=1}^{q_{max}} \frac{n_q T_i}{\tau_{T_i}} \approx T_i \sum_{q=1}^{q_{max}} \frac{n_q}{\tau_q} \quad ,$$

thus T_i is approximately given by

$$T_i \approx T_e \frac{\nu_{ei}}{n_0 < \sigma v >_{0\to 1}^{ion}} \quad . \tag{23}$$

• peak of CSD: from equation (18) neglecting the charge exchange, it is possible to obtain the derivative of the ion current,

$$\frac{(\Delta I)_{q-1}}{I_{q-1}} \approx \frac{n_q}{n_{q-1}} - 1 \simeq \frac{\tau_p - \tau_{ion}}{\tau_{ion}(1 + \tau_p n_e < \sigma v >_{q\to q+1}^{ion})} \quad ,$$

$\tau_{ion} = (n_e < \sigma v >_{q-1\to q}^{ion} - n_e < \sigma v >_{q\to q+1}^{ion})^{-1}$ is the ionization time for charge state q.
If q_M is the charge state of the most abundant current of the CSD (figure 12), the sign of the derivative $(\Delta I)_{q-1}$ has the following meaning:
-$(\Delta I)_{q-1} > 0$, $\tau_p > \tau_{ion}$, the ion confinement time is larger than the ionization time and $q < q_M$.
-$(\Delta I)_{q-1} < 0$, $\tau_p < \tau_{ion}$, the ion confinement time is lower than the ionization time and $q > q_M$.

1.3.4 Design and performance of existing ECRIS

None of the ECRIS today in operation can pretend having the full benefit of the better understanding of the physics and theory that has been presented above. The importance of several parameters is still unclear and puzzling when designing a source. Thus the choice of some parameters often results from a cost compromise rather than from a physics issue, e.g. for instance the dimensions of the source: the radial magnetic field at the chamber wall, usually created by permanent magnets, has often imposed the diameter of the chamber. The design of existing sources is sometimes already old, and new principles or concepts have not always direct applications. Although the development of new ideas is very active, the performances improve at a slower pace: (i) the technology requirements of new methods are not always easy to integrate, some advantages of the ECRIS technology, such as simplicity and compacity, may become drawbacks; (ii) most laboratories involved in ECRIS development are dependent of accelerator facilities, and are often compelled by priority to supply the accelerators highly charged ion beams rather than working on source development. This chapter surveys the main existing sources, design and specific aspects as well as performance; they are sorted out in three categories: classical, superconducting, only permanent magnet built-in sources.
More than 50 ECRIS are now in operation, the table I gives the main parameters of only a few sources shortly described below.

Most sources utilize electro-magnetic coils for the axial field, and permanent magnets for the radial hexapolar field. A few representative ion beam intensities are given in table II for some gases and in table III for some metals; various techniques for metallic ions are described in references [42]. The data given in tables II and III are not homogeneous, simply indicative although somewhat restrictive: various techniques have been set up and any comparison between these datas would be meaningless as some working conditions (extraction aperture, extraction voltage, electron sources, two-frequency heating ?, etc...) may be quite different.
Figure 13 shows the sketch of the 14 GHz AECR built at LBL [43]. The engineering design of this source differs from others essentially by the radial pumping slots in the main chamber. But whether this explains its good performance is not yet clear. Its efficient internal electron sources, and perhaps consequently its low plasma potential recently put in evidence [13] are more likely its main advantages. The peak performance is high despite its relatively low magnetic field, which makes it possible further progress. The two-frequency heating effect which was recently tested [44] has actually boosted the performances (see argon, bismuth and uranium data in tables II and III).
The 18 GHz Minimafios source has a higher magnetic field, it generally worked with gas mixing and a biased disk. Like the AECR source, its long axial dimension allows a higher ion confinement time, which may also explain its good performance for highly charged ions. This source has been now shut down [14][22].
The 14 GHz Caprice source shown in figure 14 is the last version of the first compact in size sources, as initially designed by B.Jacquot [3][45]. Its performance is still improving [29]. This high magnetic field source offers an outstanding compromise between the so many desirable characteristics of an ECRIS: high charge states, high intensities especially at medium charge states, high stability, reliability, simplicity and modularity in the design (easy access for changing parts). The best performances are obtained with an aluminum chamber [46] (see argon and uranium data in tables II and III).
The 14 GHz ECR4 source built at GANIL [47] is also a compact source which follows the main features of Caprice (figure 15), however with a stronger iron yoke. The recent version ECR4M able to work at 18 GHz [48] has interesting performances at 14 GHz (see argon data in table II).
The 10 GHz Riken ECR ion source likely one of the largest volume classical sources, is worth noticing as to the various studies of electron sources being performed [12][16][17].
The measured emittances of these classical sources usually vary in between 50π and 150π mm.mrad (for about 80% of the beam intensity) for charge states below 10; at higher charge states the emittance gets better because of the increased ion velocity, but also because the high charge state ions are actually originating from the plasma center along the main axis owing to the electrostatic ion confinement.

Until recently this demanding technology did not reach the performance of the best classical sources; it was considered to be the solution for reducing the huge power consumption of the Supermafios hexapole [2]. Today four superconducting sources have been built. The Ecrevette and Ecrevis sources of Louvain-la-neuve [49] have been already shut down. The Jülich 14.4 GHz source [50] has been successfully running for many years at the field of 0.7 T, its performance was better than other sources for very highly charged ions, likely owing to the large size facility. Actually good results of superconducting sources were only recently given by the SCECR source (figure 16) at NSCL/MSU. The SCECR works at 6.4 GHz (see tables I, II and III) in the so-called high-B mode [51], a high axial magnetic field, steep axial field gradients, a configuration actually similar to that of the compact sources Caprice and ECR4, but the radial hexapolar field. Interestingly this source has good performance for very highly charged states, and its next operation step at 14 GHz with a higher hexapole field is expected to be really promising, and hopefully a breakthrough. It is likely that higher performance of the SCECR at 14 GHz will be obtained by using more intense cold electron sources than ~~in the today operation~~, because of the large size plasma volume and the higher electron density.

1.3.4.3 Only permanent magnet built-in sources

Although limited in performance and delivering medium charge states, these sources are worth mentioning: both axial and radial magnetic fields are obtained only with permanent magnets. The lack of axial field tuning is compensated by the miniaturization and a reduced power consumption, only that of the rf generator. This advantage together with their high simplicity and flexibility make them quite attractive to high voltage platform accelerators. The 8 GHz Neomafios source built by the Grenoble group [52] has been extensively used at the Riken Institute in Japan with as many as 47 different elements [53]. A 10 GHz version of Neomafios [54] with improved performance is now working at the Osaka University RCNP [55], it can deliver Ar^{11+} 5eμA – Ar^{8+} 100eμA beams. A quite compact source, Nanogan 10 GHz, built by the Ganil group [56] for on-line production of radioactive ions, delivers Ar^{11+} 3eμA – Ar^{8+} 60eμA beams; it is quite remarkable by its low weight and small size as well as its low rf power consumption.
Owing to high quality permanent magnets (FeNdB) new compact sources are being designed, and one may soon expect interesting performance sources in this field [57]. Another challenge is the use of the small size-low cost 2.45 GHz rf generators for ECRIS at high voltage, several prototypes are already in operation with modest performance.

1.3.5 Prospects of development for ECRIS

This chapter summarizes the current thinking on the main issues for further advances of ECRIS performance, and surveys the new concepts

1.3.5.1 Main issues for future ECRIS

Despite the compromise between intensity and charge state in the ECRIS, there are still possibilities of improved performance. The previous chapters suggest the dominant trends and issues for future ECRIS: improved magnetic configuration, reinforced electron cyclotron heating, and enhanced electron sources to supply enough cold electrons to the plasma. Higher charge states and higher intensities clearly require improved particle confinement times τ_e and τ_q, so as to build high electron density plasmas efficient for ionization and confining highly charged ions as well as possible.

Accordingly this leads to high magnetic fields (both radial and axial), high mirror ratios, and also to high rf frequencies in order to fit in with the resonance condition (1). The evidence that higher magnetic fields lead to higher performance is almost general, but the most impressive example is given by the SCECR source at MSU [51]. The question whether there is an intrinsic effect of the rf frequency itself, such as a shielding effect of rf waves by the plasma [2], is still not clear, but the current idea is now that the gains originally credited to a frequency scaling as that of formula (7) may have been actually due to the increase of magnetic field strength.

The impressive results obtained with two-frequency heating in the AECR source at LBL [44] have suggested the MF-ECR concept [58], or Multiple Frequency ECR source, as an extension to several frequencies of the two-frequency heating in a magnetic configuration with high magnetic fields and high mirror ratios: closed ECR heating surfaces, nested in each other, could be simultaneously produced at 10, 14 and 18 GHz (these frequencies being commercially available), and would drastically reinforce the electron heating and the plasma confinement, thus improving the source performance.

At last more intense electron sources are desirable in order to reach a higher electron density: aluminum as a plasma chamber material is a good candidate for doing so, it forms a resistant oxide layer that has a high secondary emission coefficient [58], this technique has given excellent results in the Caprice source [46]. Besides an intense electron source is reported to improve the plasma stability and to reduce the plasma potential ϕ [13].

Together with a higher electron density, a larger size plasma is expected to allow a better ion confinement. This in turn should reduce the neutral density within the plasma by neutral burn-up, and hopefully the charge exchange losses, today the dominant limiting mechanism of high charge state ion production.

The electron temperature control does not seem to be a critical issue so far. However the respective roles of the two quasi-maxwellian, bulk and tail, components of the electron population need to be understood.

Regarding the design requirements of the above issues, only superconducting ECRIS (axial and hexapolar coils) can reach the necessary multi-Tesla fields. Optimized rf coupling systems [11] will be also necessary for

1.3.5.2 New ECRIS under construction and concepts

The SERSE project [59], a superconducting source being built by the CEA/DRFMC-Grenoble in a joint venture with the INFN/LNS-Catania, is expected to confirm the main issues described above. The SERSE source is designed in order to reach the highest magnetic fields so far used in ECRIS, 1.4 T radially at the chamber wall and 2.7 T axially at the mirror throat with a mirror ratio R_z as large as 6.0. A sketch of the magnet system is shown in figure 17, the central coil works with reverse field, the mirror-to-mirror length is 50 cm and the plasma chamber diameter 13 cm. At 14.5 GHz the expected performance of SERSE is 1 eμA of Si^{14+}, Ar^{17+}, Kr^{29+}, and Xe^{40+} ion beams. Further operation of SERSE at 30 GHz with gyrotron tubes is also planned.
A new 18 GHz ECRIS at Riken [60] has just started. It is a high magnetic field source, 1.4 T axially and radially, of classical technology, coils and permanent magnets, although the hexapole design is quite specific. The source dimensions are similar to those of Minimafios. The source should be flexible enough so as to tailor the mirror ratio and the axial magnetic field gradient without changing the peak field strength. Preliminary results look quite promising
A new concept of ECRIS recently proposed is under study [61]. Basically this concept is defined as a "volume"ECR zone source, whereas today ECRIS are "surface"ECR zone sources, which means that the whole plasma volume lying in a magnetic well with a flat bottom is everywhere in resonance with the rf waves. This concept would offer noticeable improvements as to the rf power absorption and particle confinement.

Acknowledgments

The authors acknowledge the help and advices of their Grenoble colleagues in preparing this review article.

References

[1] T.C.Simonen, Proc. IEEE **69**, 935 (1981).

[2] R.Geller, Europhys. News **22**, 8 (1991); R.Geller, Annu. Rev. Nucl. Part. Sci. **40**, 15 (1990); R.Geller, IEEE Trans. Nucl. Sci. **NS-23**, 904 (1976); R.Geller, ibid. **NS-26**, 2120 (1979).

[3] B.Jacquot, F.Bourg, R.Geller, Nucl. Instrum. Meth. **A254**, 13 (1987); B.Jacquot, M.Pontonnier, ibid. **A287**, 341 (1990) and ibid. **A295**, 5 (1990).

[4] J.Vámosi and S.Biri, to be published in Nucl. Instrum. Meth. **B**(1994).

[5] G.Melin et al., Rev. Sci. Instrum. **61**, 236 (1990).

tional Workshop on ECRIS, Riken, April 25-27, 1995.

[7] F.Jaeger, A.J.Lichtenberg and M.A.Lieberman, Plasma Physics, **14**, 1073 (1972); M.A.Lieberman and A.J.Lichtenberg, ibid., **15**, 125 (1973); A.J.Lichtenberg, M.J.Schwartz and D.T.Tuma, ibid., **11**, 101 (1969).

[8] A.Girard, Proc. ECRIS 11, Report N° KVI 996 Groningen, 86 (1993).

[9] T.H.Stix, Waves in Plasmas, American Institute of Physics, New York (1992).

[10] C.Lyneis, Proc. 13th Int. Conf. Cycl. Appl. Vancouver, World Scientific, editors G.Dutto and M.K.Craddock, 301 (1992).

[11] G.Melin et al., to be published in Proceedings of the 12th International Workshop on ECRIS, Riken, April 25-27, 1995.

[12] T.Nakagawa et al., Jpn. J. Appl. Phys. **32**, 1335 (1993).

[13] Z.Q.Xie and C.M.Lyneis, Proc. ECRIS 11, Report N° KVI 996 Groningen, 106 (1993); Rev. Sci. Instrum. **65**, 2947 (1994).

[14] G.Melin et al., Proc. ECRIS 10, Report N° ORNL CONF-9011136, 1 (1990).

[15] Z.Q.Xie, C.M.Lyneis, R.S.Lam, and S.A.Lundgren, Rev. Sci. Instrum. **62**, 775 (1991).

[16] T.Nakagawa, Jpn. J. Appl. Phys. **30**, 930 (1991).

[17] T.Nakagawa and T.Kageyama, Jpn. J. Appl. Phys. **30**, 1588 (1991); T.Nakagawa et al., ibid. **31**,1129 (1992).

[18] W.Lotz, Z. Physik **206**, 205 (1967); ibid. **216**, 241 (1968); ibid. **220**, 466 (1969); ibid. **232**, 101 (1970).

[19] R.Harkewicz et al., to be published in Proceedings of the 12th International Workshop on ECRIS, Riken, April 25-27, 1995.

[20] H.Tawara and T.Kato, Atomic Data and Nuclear Data Tables **36**, 167 (1987).

[21] M.O.Krause and T.A.Carlson, Phys.Rev. **158**, 18 (1967).

[22] C.Barué, P.Briand, A.Girard, G.Melin, and G.Briffod, Rev. Sci. Instrum. **63**, 2844 (1992).

[23] C.Barué, M.Lamoureux, P.Briand, A.Girard, G.Melin, J. Appl. Phys. **76**, 2662 (1994).

[24] A.Girard et al., Rev. Sci. Instrum. **65**, 1714 (1994).

[25] F.F.Chen, Introduction to Plasma Physics and Controlled Fusion, 2nd ed., Plenum Press, New York (1984).

ers, New York (1967).

[27] J.W.Shearer, Report N° UCID-19577 LLNL (1982).

[28] R.C.Gardner, Ph.D. thesis, Report N° MIT/PFC/RR-86-23 (1986).

[29] D.Hitz, G.Melin, M.Pontonnier, T.K.Nguyen, Proc. ECRIS 11, Report N° KVI 996 Groningen, 91 (1993).

[30] D.R.Whaley, W.D.Getty, Phys. Fluids B **2**, 1195 (1990).

[31] V.P.Pastukhov, Nucl. Fusion **14**, 3 (1974).

[32] P.Sortais, Rev. Sci. Instrum. **63**, 2801 (1992).

[33] P.Briand, R.Geller, G.Melin, Nucl. Instrum. Meth. **A294**, 673 (1990).

[34] M.Delaunay, Rev. Sci. Instrum. **63**, 2861 (1992).

[35] T.A.Antaya, J. Phys. (Paris), Colloque C1 **50**, 707 (1989).

[36] A.G.Drentje and J.Sijbring, Proc. ECRIS 10, Report N° ORNL CONF-9011136, 17 (1990); A.G.Drentje, Rev. Sci. Instrum. **63**, 2875 (1992); A.G.Drentje et al., to be published in Rev. Sci. Instrum., Proc. 6th ICIS, Vancouver, Sept 11-15, 1995.

[37] Z.Q.Xie, private communication (1994).

[38] Y.Jongen, Reports N° LC-8001 and N° LC-8003, Université Catholique de Louvain (1980).

[39] S.Bliman and N.Chang-Tung, J. Phys. (Paris) **42**, 1247 (1981).

[40] H.I.West, Report N° UCRL-53391 LLNL (1982).

[41] J.H.Booske, F.Aldabe, R.F.Ellis and W.D.Getty, J. Appl. Phys. **64**, 1055 (1988); S.Pešić and M.Vuković, Phys. Rev. A **42**, 3571 (1990); G.D.Shirkov, Plasma Sources Sci. Technol. **2**, 250 (1993).

[42] R.Geller, P.Ludwig and G.Melin, Rev. Sci. Instrum. **63**, 2795 (1992); R.Harkewicz, J.Stacy, J.Greene and R.Pardo, ibid. **65**, 1104 (1994).

[43] C.M.Lyneis, Z.Q.Xie, D.J.Clark, R.S.Lam and S.A.Lundgren, Proc. ECRIS 10, Report N° ORNL CONF-9011136, 47 (1990).

[44] Z.Q.Xie and C.M.Lyneis, to be published in Rev. Sci. Instrum. (1995).

[45] B.Jacquot and M.Pontonnier, Proc. ECRIS 10, Report N° ORNL CONF-9011136, 133 (1990); D.Hitz, B.Jacquot, R.Geller, M.Pontonnier and F.Bourg, ibid., 173 (1990).

[46] D.Hitz et al., to be published in Proceedings of the 12th International Workshop on ECRIS, Riken, April 25-27, 1995; to be published in Rev. Sci. Instrum., Proc. 6th ICIS, Vancouver, Sept 11-15, 1995.

55 (1990).

[48] R.Leroy et al., to be published in Proceedings of the 12th International Workshop on ECRIS, Riken, April 25-27, 1995.

[49] Y.Jongen, C.Pirart, G.Ryckewaert, Proc. ECRIS 4, internal report CENG, 3.1 (1982).

[50] H.Beuscher, Rev. Sci. Instrum. **61**, 262 (1990).

[51] T.A.Antaya, S.Gammino, Rev. Sci. Instrum. **65**, 1723 (1994); T.A.Antaya et al., Proc. 3rd Int. Conf. Radioac. Nucl. Beams East Lansing, May 1993.

[52] P.Sortais et al., Proc. ECRIS 8, Report N° NSCL # MSUCP-47 East Lansing, 334 (1987).

[53] T.Nakagawa et al., Proc. 9th Symp. Acc. Sci. Techn. Tsukuba, 4 (1993).

[54] P.Ludwig, R.Geller, and G.Melin, Rev. Sci. Instrum. **63**, 2892 (1992).

[55] M.Tanaka et al., to be published in Phys. Rev. A (1994).

[56] P.Sortais et al., Proc. ECRIS 11, Report N° KVI 996 Groningen, 97 (1993).

[57] P.Sortais et al., to be published in Proceedings of the 12th International Workshop on ECRIS, Riken, April 25-27, 1995.

[58] C.M.Lyneis and Z.Q.Xie, to be published in Proceedings of the 12th International Workshop on ECRIS, Riken, April 25-27, 1995.

[59] G.Ciavola and S.Gammino, P.Briand, G.Melin and P.Seyfert, Rev. Sci. Instrum. **65**, 1057 (1994); see also Proc. EPAC 94 London **2**, 1421 (1994).

[60] T.Nakagawa et al., Proc. 9th Symp. Acc. Sci. Techn. Tsukuba, 19 (1993).

[61] G.D.Alton, Rev. Sci. Instrum. **65**, 775 (1994); to be published in Proceedings of the 12th International Workshop on ECRIS, Riken, April 25-27, 1995.

Fig.1. Sketch of the design of an ECR ion source.
Fig.2. (a) ECRIS magnetic flux tube created by an axial mirror field and a radial hexapolar field. (b) guiding center trajectories of electrons confined within the resonance surface from [4]. (c) magnetic isobars of the Quadrumafios source from 0.5 Tesla (min) to 0.78 Tesla (max) from [6].
Fig.3. Electron energy versus normalized time for different initial phases, showing the resonance crossings and the stochastic heating from [7].
Fig.4. Argon ionization rates from the convolution of the Lotz formula with a maxwellian electron distribution function.
Fig.5. Bulk electron temperature versus rf power from the 10 GHz Quadrumafios facility [24].
Fig.6. Total electron density (in 10^{12}cm^{-3}) versus rf power from the 10 GHz Quadrumafios facility [24].
Fig.7. Tail electron temperature versus rf power from the 10 GHz Quadrumafios facility [24].
Fig.8. Magnetic field squared (Gauss) of mass spectrometer versus source bias (V) giving by least square fit the plasma potential ϕ from [13].
Fig.9. Postulated plasma potential along the axis of the confinement region of an ECR ion source from [40].
Fig.10. Ar^{8+} ion current versus input rf power at different optimized rf powers from the Caprice source [29].
Fig.11. Afterglow pulses versus time (ms): (a) Au^{27+} ion current (eμA) [29], (b) Pb^{28+} ion current (eμA) [32].
Fig.12. Argon charge state distribution of currents (eμA) of the 14 GHz Caprice source tuned on Ar^{16+} from [46].
Fig.13. Elevation view of the AECR source [43].
Fig.14. Elevation view of the high B Caprice source: 1-permanent magnet hexapole, 2-solenoid coils, 3-closed $|B|$ surfaces, 4-rf power input, 5-gas inlet, electric oven feedthroughs, 6-ion extraction [29].
Fig.15. Elevation view of the ECR4 source [47].
Fig.16. Cutaway view of the SCECR source [51].
Fig.17. Hexapole and solenoidal coils of the SERSE source [59].

Table captions

Table I. Today operating parameters of a few ECRIS: maximum axial field B_z^{max}, maximum axial mirror ratio $R_z = B_z^{max}/B_z^{min}$, hexapole magnetic field at wall B_r^{wall}, axial mirror to mirror distance L_z, plasma chamber diameter d, power consumed by the axial coils P_{coils}.
Table II. A few representative (best known data) ion currents (eμA) from different sources for gases, cw regime.
Table III. A few representative (best known data) ion currents (eμA) from different sources for metals, cw regime.

AECR	10500	2.6	6400	~40	7.0	<90
Minimafios	14400	2.7	7200	35	7.0	160
Caprice	14500	3.5	10500	21	6.6	60/70
ECR4	11000	2.8	9000	~20	6.6	50
Riken	~6000	1.8	–	50	10	–
SCECR	12500	7.3	4400	50	14	~0

Table II

ion	AECR	Minimafios	Caprice	ECR4	Riken	SCECR
O^{6+}	>500	800	1130	1000	150	840
O^{7+}	>150	180	190	–	60	185
Ar^{8+}	–	–	680	600	–	370
Ar^{11+}	>160	140	185	–	80	170
Ar^{13+}	59	45	34	–	12	56
Ar^{14+}	33	20	17	15	8	30
Ar^{16+}	4	1.4	1	–	0.8	2.1
Ar^{17+}	–	0.02	–	–	–	–
Ar^{18+}	–	0.001	–	–	–	–
Kr^{17+}	100	32	70	50	31	100
Kr^{19+}	77.5	22	25	20	16	65
Kr^{20+}	57.5	15	15	8.5	8.5	43
Kr^{21+}	40.5	9	7	–	–	27
Kr^{23+}	18.5	3	2	–	–	7
Kr^{24+}	11	2	–	–	–	5.1
Xe^{22+}	48	–	40	30	–	78
Xe^{25+}	68	–	32	17	–	55
Xe^{27+}	37.5	–	12	–	–	34
Xe^{29+}	–	–	5	3	–	4.4
Xe^{30+}	5	–	–	–	–	1.4

$Fe^{[illegible]}$	–	1	–
Au^{27+}	–	10	–
Au^{31+}	–	1.5	–
Pb^{27+}	–	20	25
Pb^{31+}	–	10	8
Pb^{36+}	–	0.3	–
Pb^{37+}	–	0.1	–
Bi^{33+}	12.1	–	–
Bi^{34+}	10.2	–	–
Bi^{36+}	6.5	–	–
Bi^{40+}	1.8	–	–
U^{27+}	–	20	10
U^{29+}	–	15	–
U^{33+}	12	5	–
U^{37+}	7.1	0.9	–
U^{39+}	3.7	0.17	–
U^{43+}	0.5	–	–

Fig 1

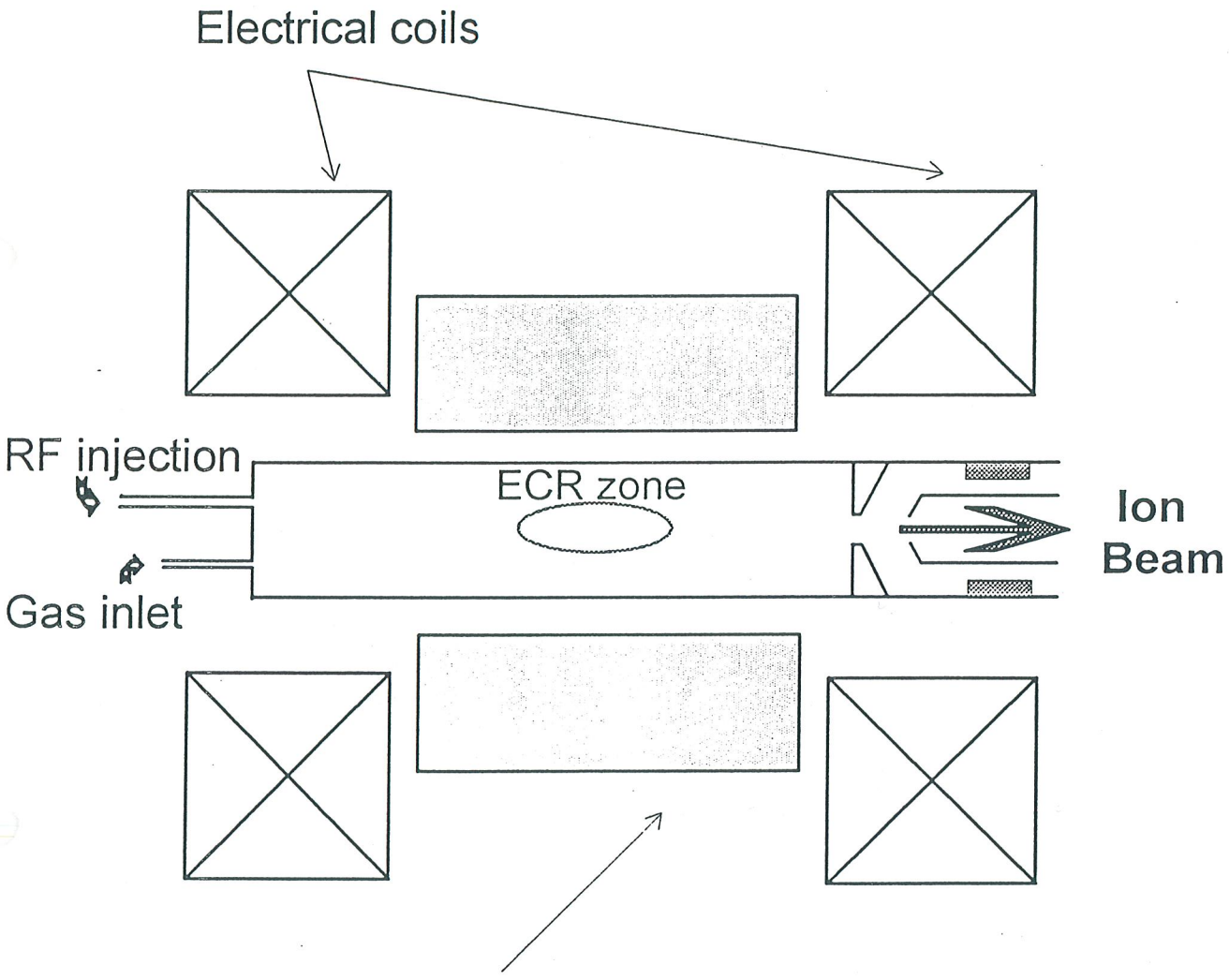
Electrical coils
RF injection
Gas inlet
ECR zone
Ion
Beam
Multipole (permanent magnets - Ioffe bars)

(a)

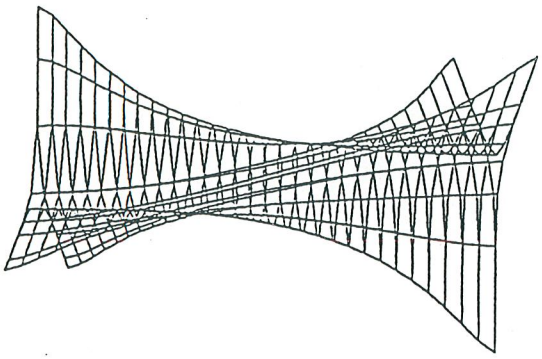

Fig 2

(b)

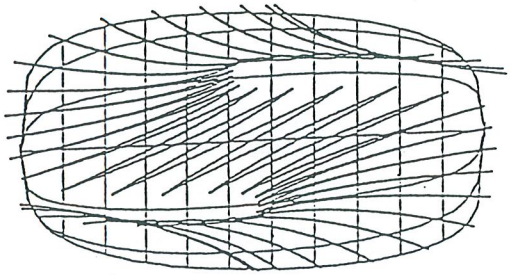

(c)

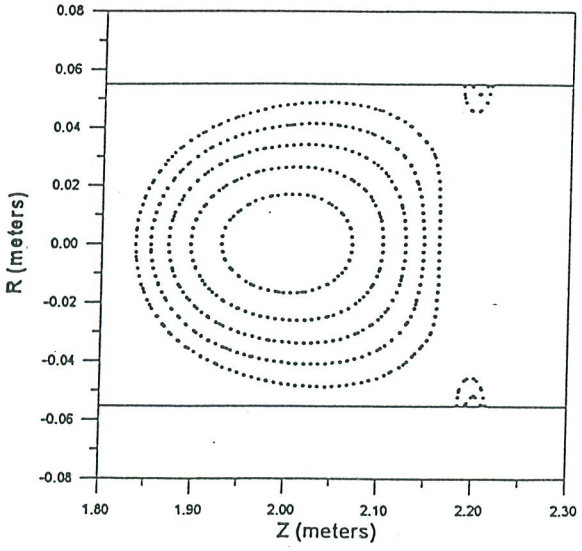
0.08
0.06
0.04
0.02
0.00
-0.02
-0.04
-0.06
-0.08
R (meters)
1.80
1.90
2.00
2.10
2.20
2.30
Z (meters)

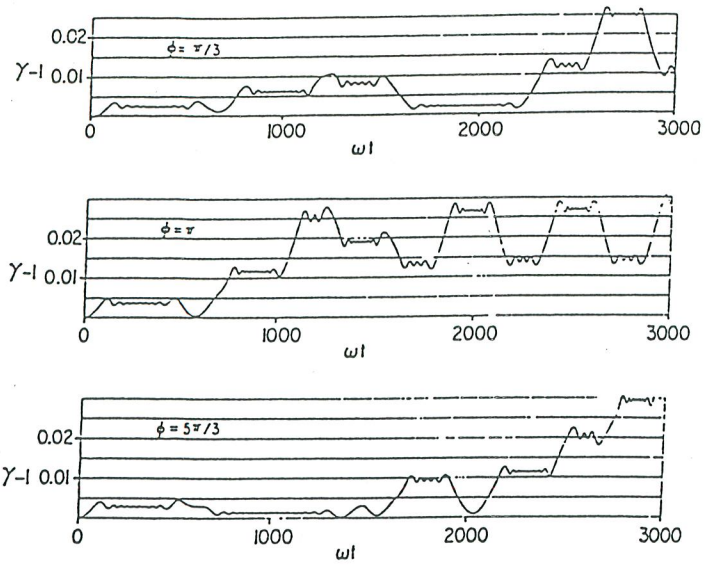

Fig 3

what are figures?

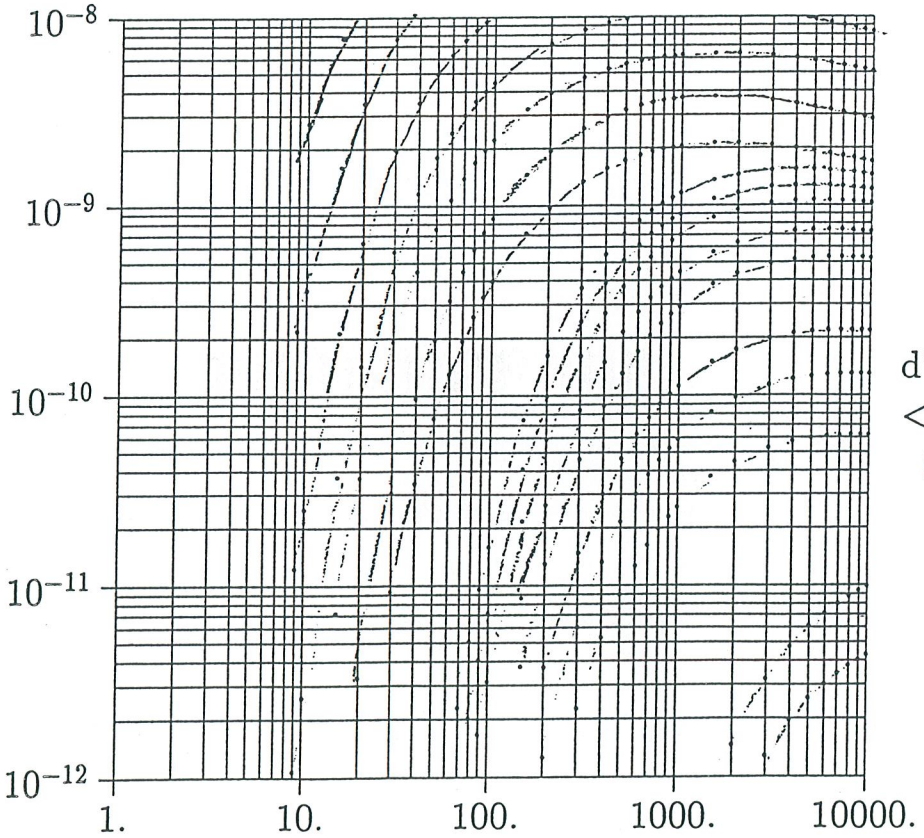

Fig 4

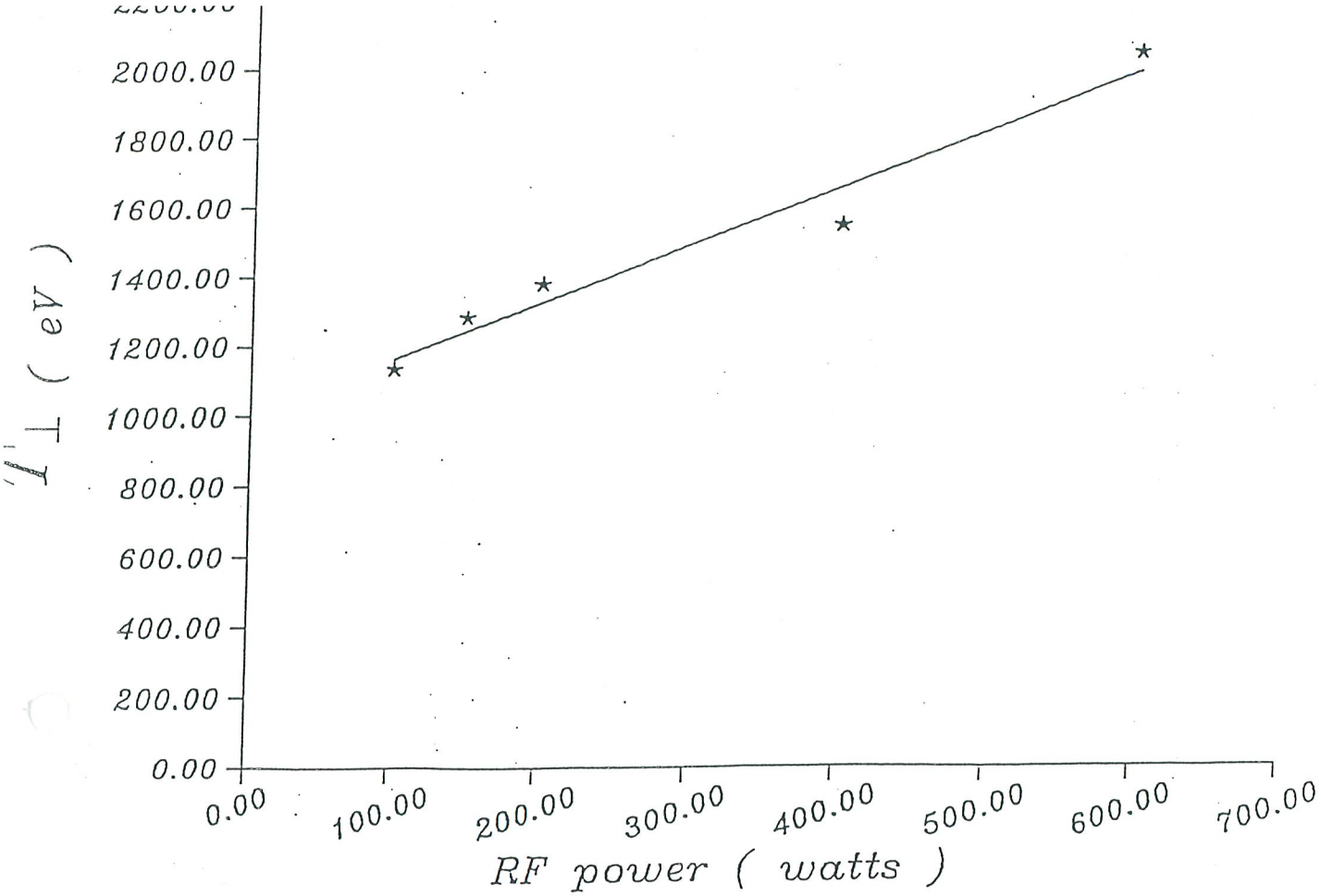
2000.00
1800.00
1600.00
1400.00
1200.00
1000.00
800.00
600.00
400.00
200.00
0.00
T⊥ (eV)
0.00
100.00
200.00
300.00
400.00
500.00
600.00
700.00
RF power (watts)

Fig 6

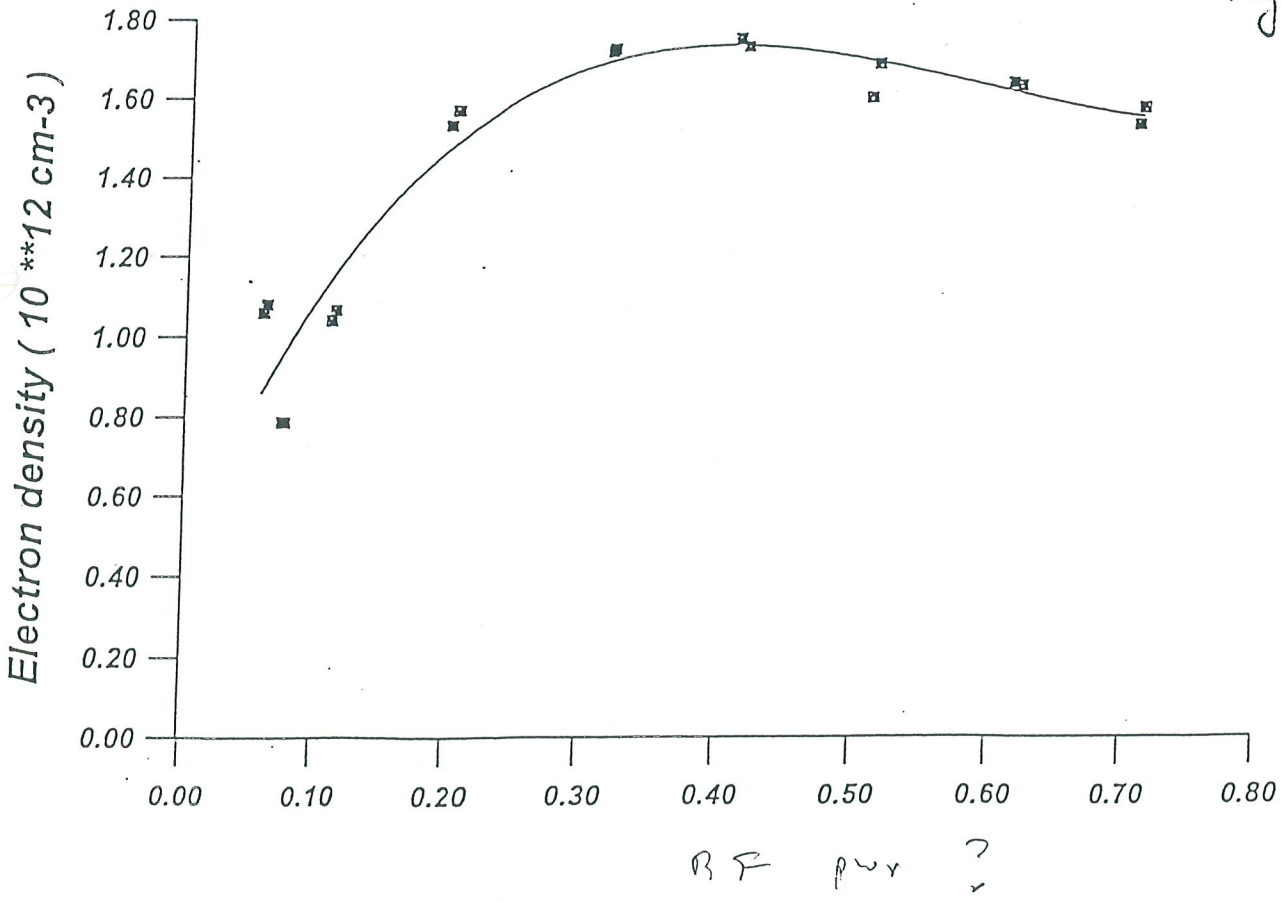
1.80
1.60
1.40
1.20
1.00
0.80
0.60
0.40
0.20
0.00
Electron density (10 **12 cm-3)
0.00
0.10
0.20
0.30
0.40
0.50
0.60
0.70
0.80
RF pwr ?

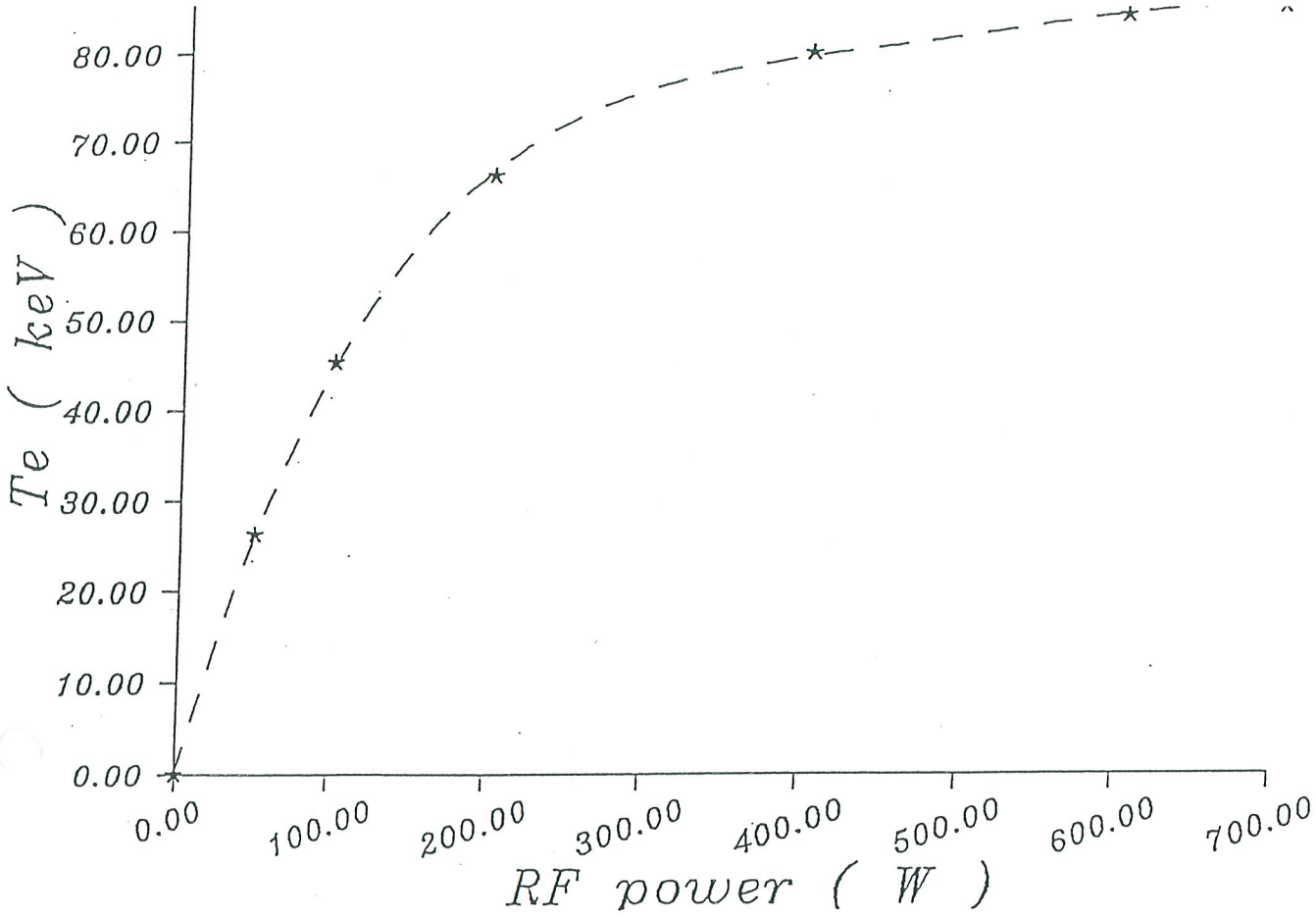
80.00
70.00
60.00
50.00
40.00
30.00
20.00
10.00
0.00
Te (keV)
0.00
100.00
200.00
300.00
400.00
500.00
600.00
700.00
RF power (W)

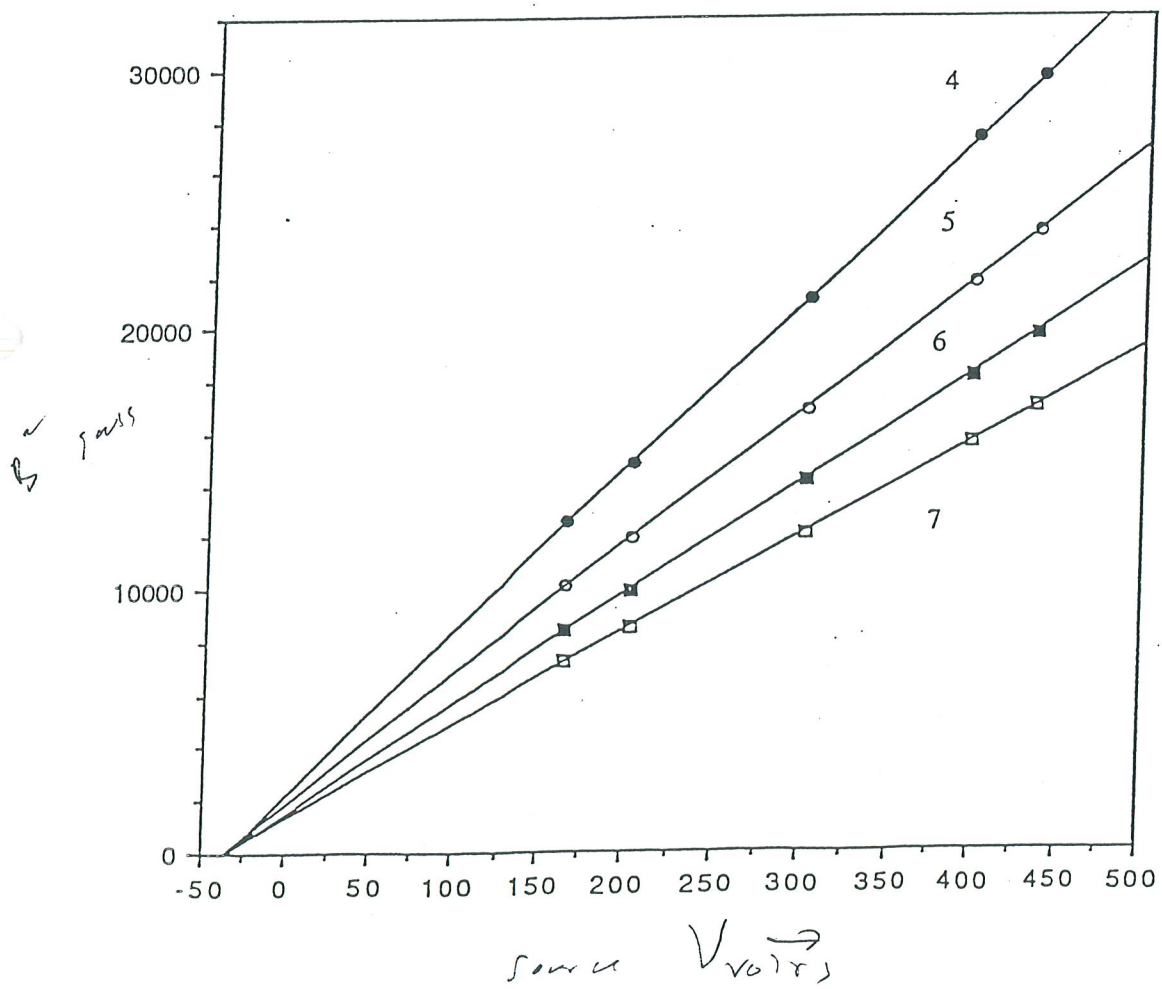
30000
20000
10000
0
4
5
6
7
-50
0
50
100
150
200
250
300
350
400
450
500
Source V volts

Fig 8

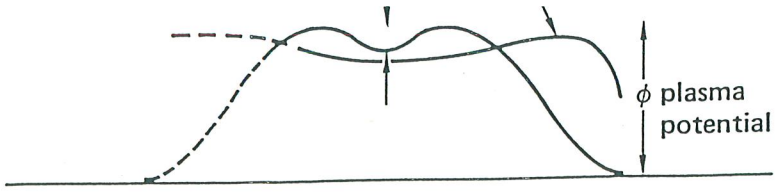

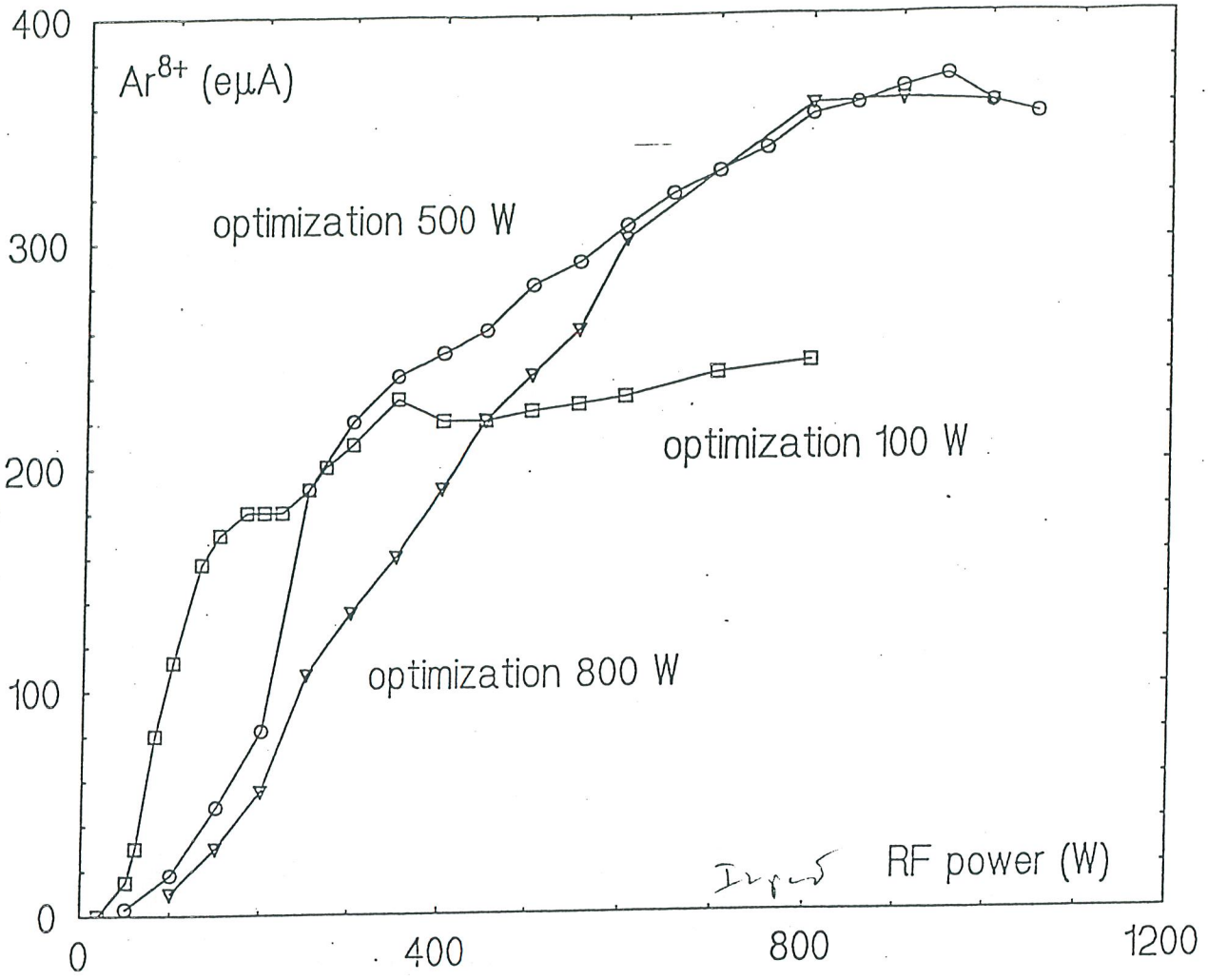

Fig 10

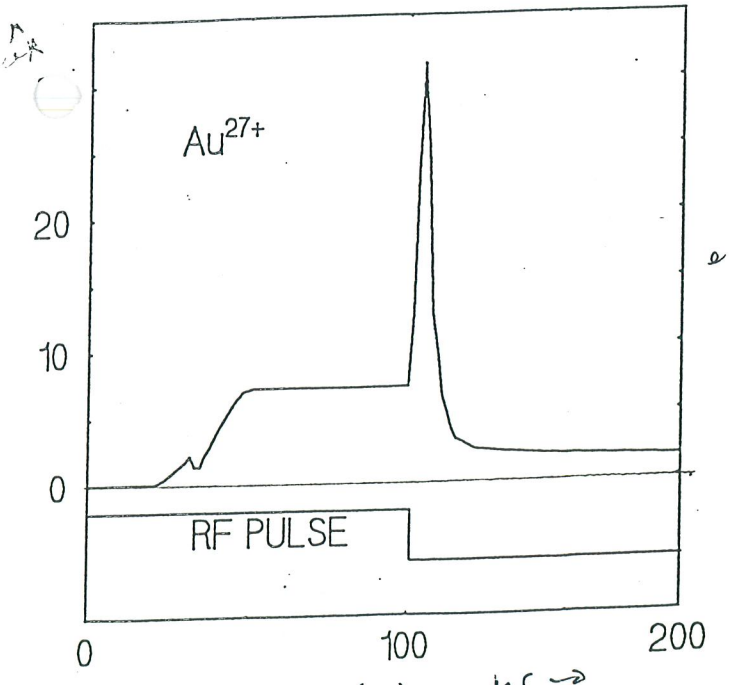

(a)

Fig 11

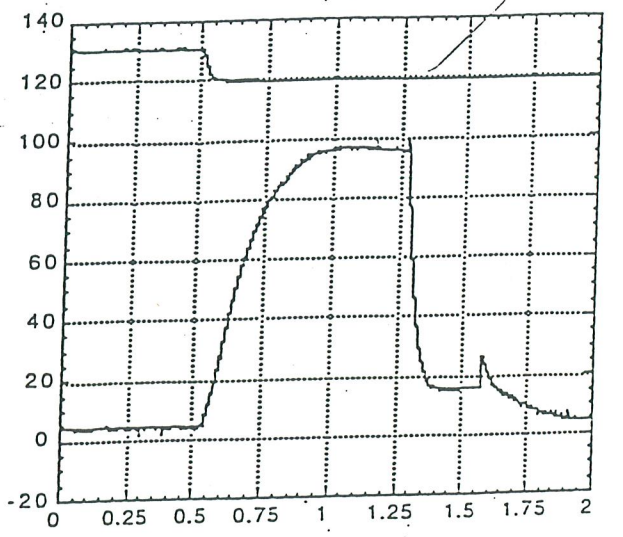

(b)

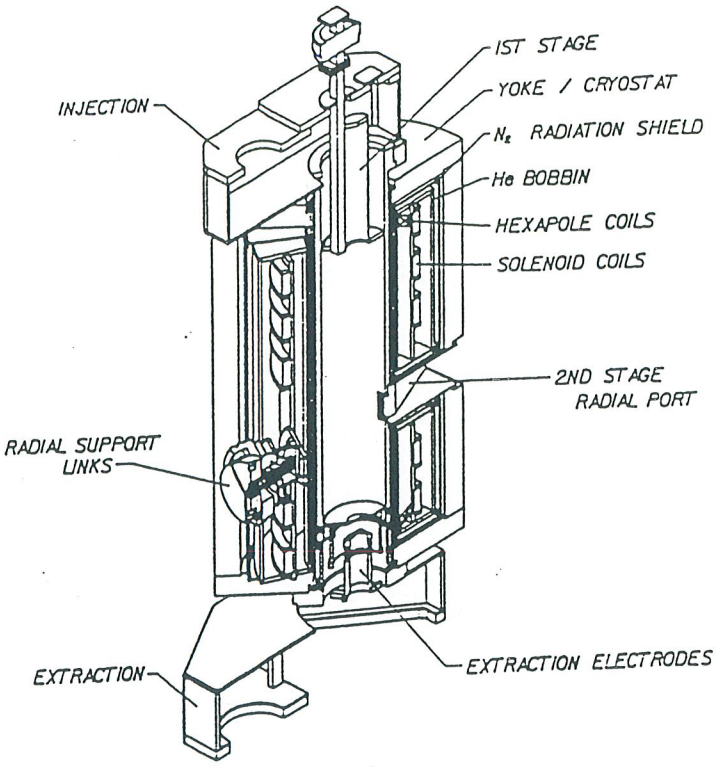
IST STAGE
YOKE / CRYOSTAT
N_2 RADIATION SHIELD
He BOBBIN
HEXAPOLE COILS
SOLENOID COILS
2ND STAGE
RADIAL PORT
RADIAL SUPPORT
LINKS
INJECTION
EXTRACTION
EXTRACTION ELECTRODES

Fig 17

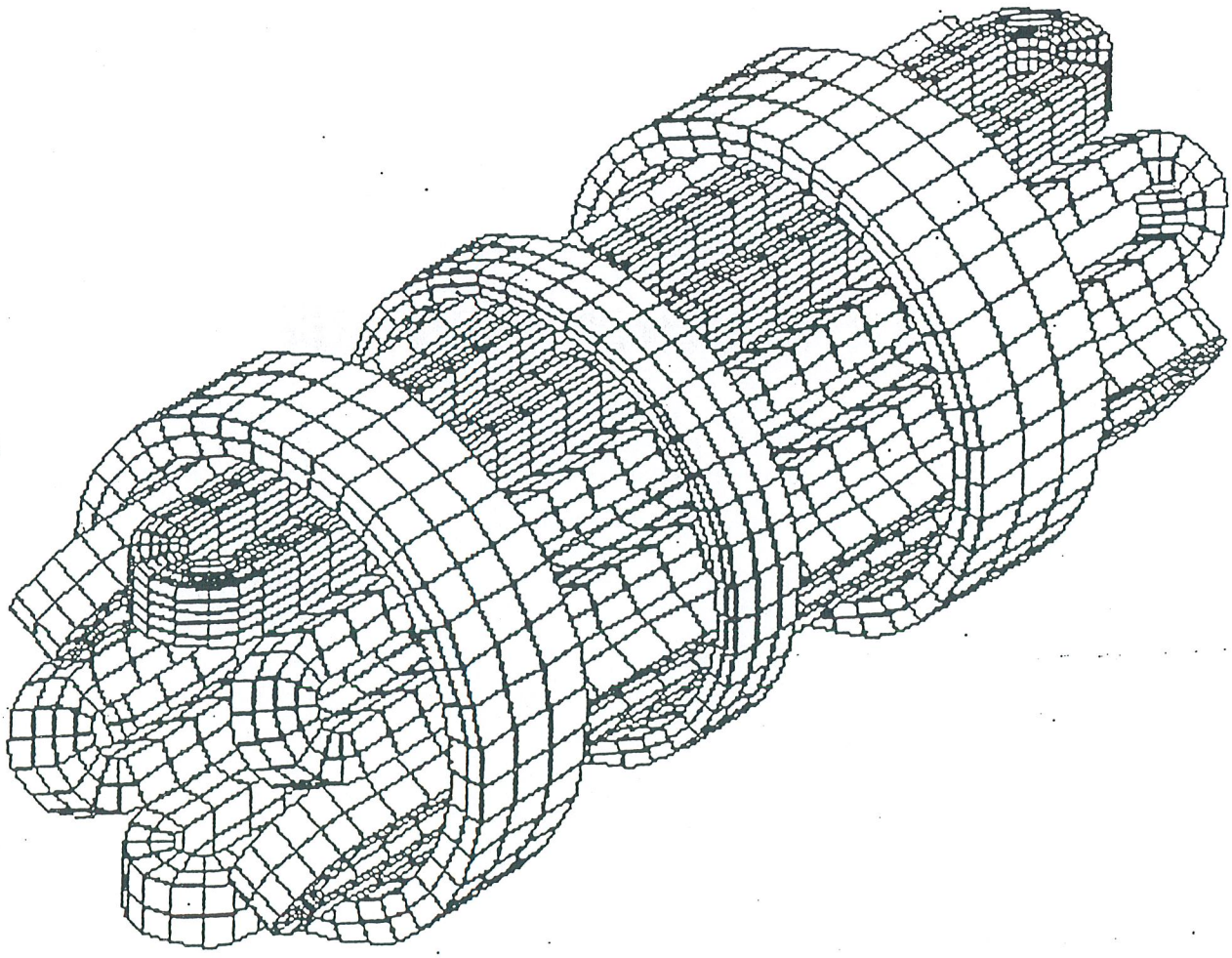

Fig 14

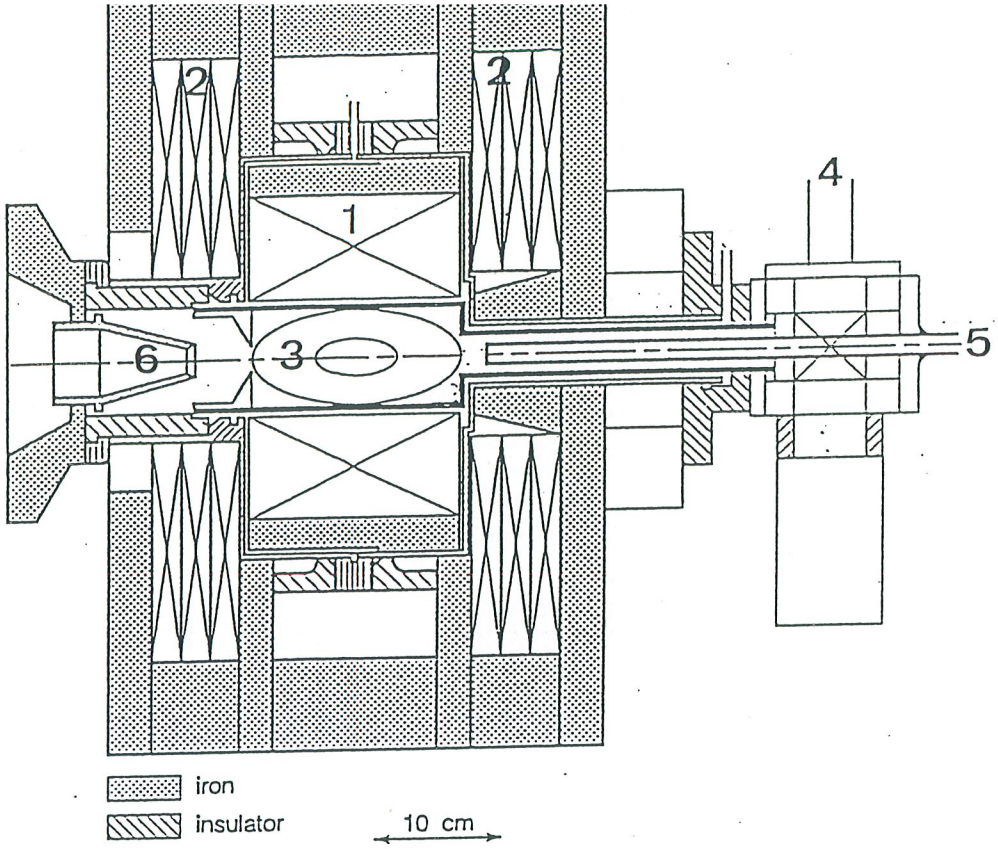
2
2
1
4
6
3
5
iron
insulator
10 cm

Fig 15

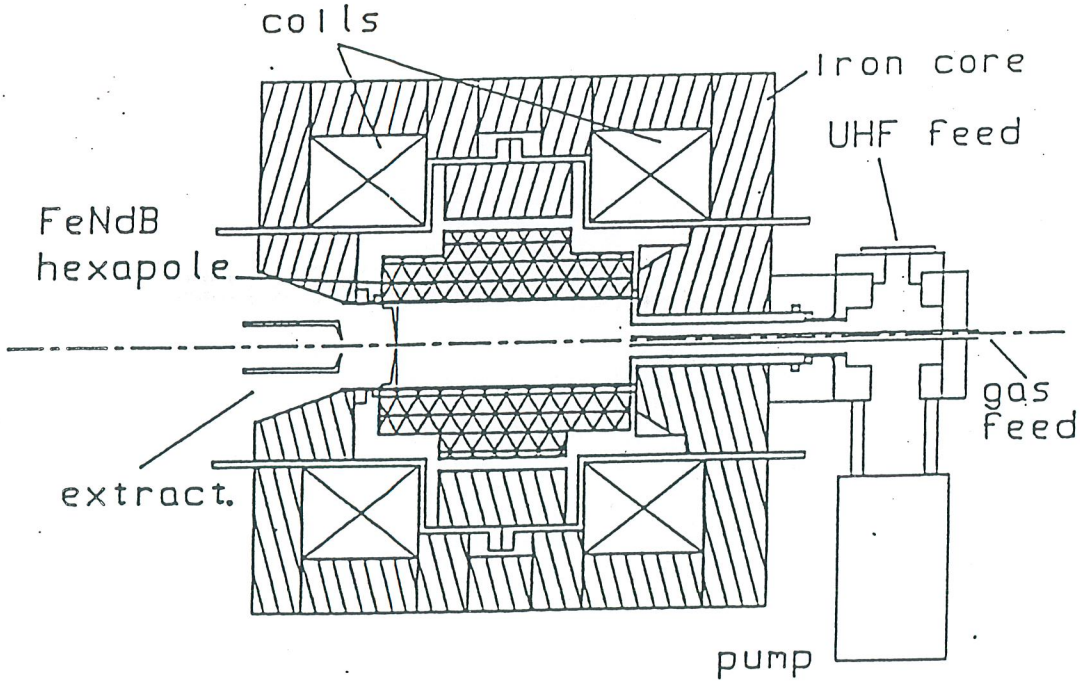
coils
Iron core
UHF feed
FeNdB
hexapole
gas
feed
extract.
pump

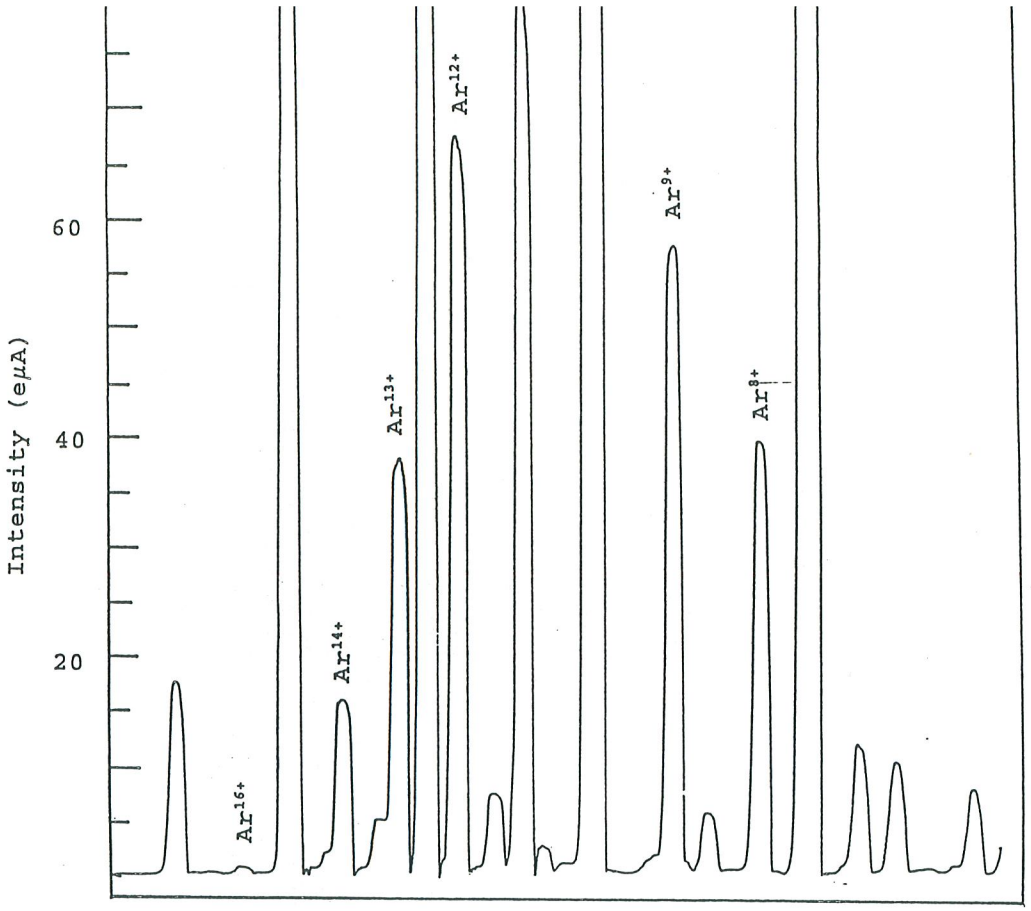
Intensity (eμA)
60
40
20
Ar16+
Ar14+
Ar13+
Ar12+
Ar9+
Ar8+

Fig 13

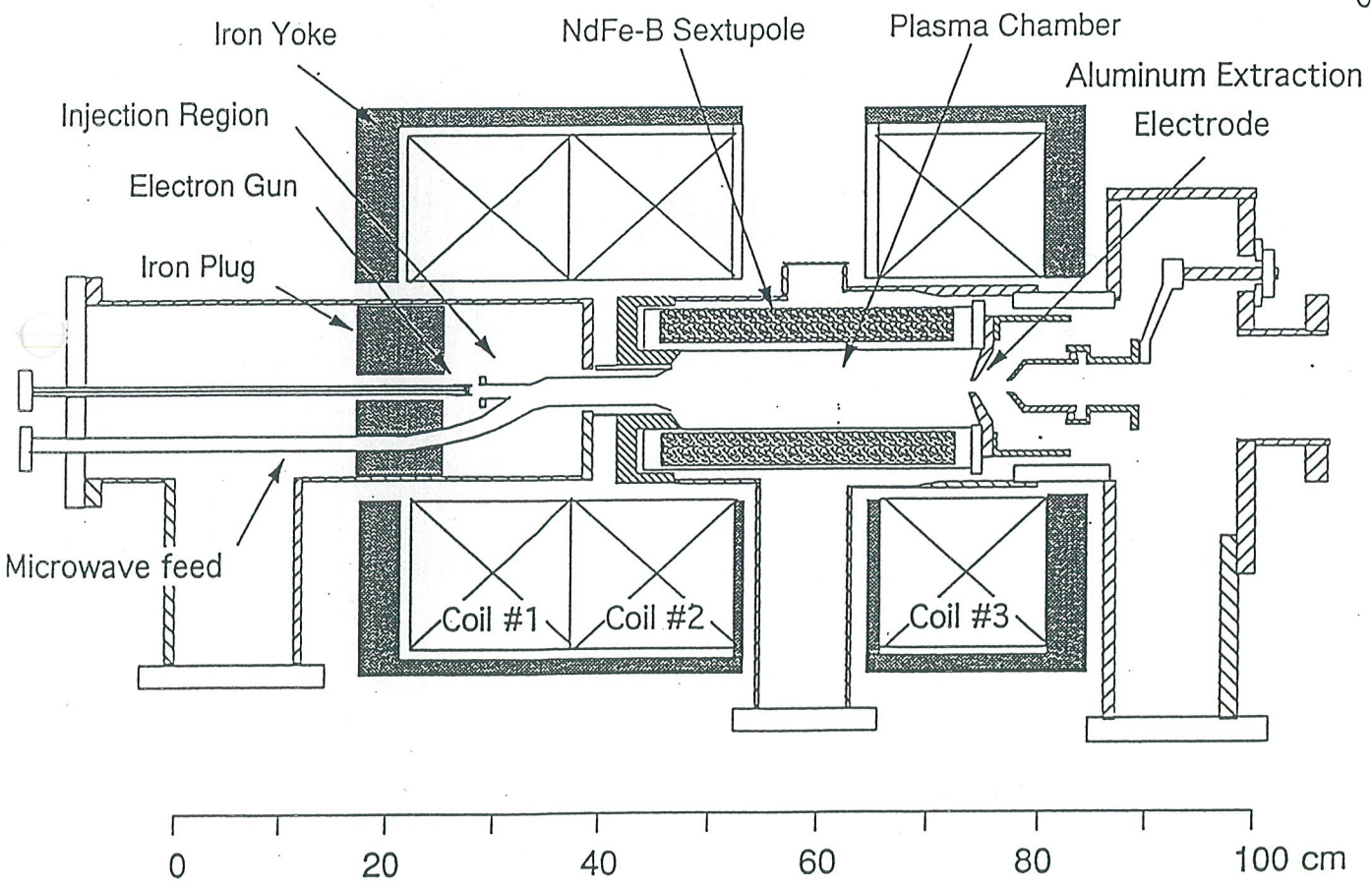
Iron Yoke
NdFe-B Sextupole
Plasma Chamber
Aluminum Extraction
Electrode
Injection Region
Electron Gun
Iron Plug
Microwave feed
Coil #1
Coil #2
Coil #3
0
20
40
60
80
100 cm